Aalto University
School of Engineering
Master's Programme in Energy Technology

Andrés Calvo Luz

Study of bubbly flows in an open-source software

Master's Thesis
Espoo, May 28, 2018

Supervisor: Ville Vuorinen, Assistant Professor
Thesis advisor: Erkki Laurila, M.Sc. (Tech.)

Aalto University
School of Engineering

Aalto University, P.O. BOX 11000, 00076 AALTO
www.aalto.fi
Abstract of the master's thesis

Author Andrés Calvo Luz

Title Study of bubbly flows in an open-source software

Degree programme Energy Technology

Major Energy **Code of major** ENG21

Supervisor Assistant Professor Ville Vuorinen

Advisor M.Sc. (Tech) Erkki Laurila

Date 28.05.2018 **Number of pages** 74 **Language** English

Abstract

Bubbly flows occur everywhere in nature and engineering. The study of such flows can be done theoretically, experimentally or computationally. In the present thesis, latter option was chosen and multiphase computational fluid dynamics (M-CFD) simulation methods are tested for simulation of a specific situation of such flows. All the simulations done under this thesis are about an initially spherical bubble starting from rest in quiescent water. In order to accurately assess the dynamics of that bubble an open-source M-CFD software was used, OpenFOAM. The dynamics of the bubble was set by means of the study of three characteristics: rise velocity, trajectory and shape. Here, a Matlab algorithm was developed to get the rise velocity of the bubble. Two cases have been simulated based on Krishna et al. (1999) experimental, simulated and numerical data base, one in two dimensions and the other in three dimensions, both were computed to a range of bubble between 4 and 12 millimeters in diameter. The simulations were carried out using a geometric Volume-Of-Fluid (VOF) method, IsoAdvector which utilizes iso-surfaces in the subcell interface reconstruction step. This algorithm provides results that are close agreement with the experimental, simulated and numerical data already named, and also in close agreement with the experimental rise velocities of Haberman et al. (1953) investigation. Furthermore, the rise velocity equation proposed by Jamialahmadi et al. (1994) and the bubble shapes shown in Kumar Tripathi et al. (2015) simulations match with the simulations of the present study. Therefore, these results verify the capability of OpenFOAM simulations with IsoAdvector algorithm, which are powerful tools for a priori determination of the morphology and rise characteristics of an initially spherical bubble starting from rest in quiescent water and yield on the same level as ANSYS-CFX commercial software.

Keywords Open-source , Rise velocity , Trajectory , Bubble shape , IsoAdvector , M-CFD

Contents

List of Figures

List of Tables

Symbols and abbreviations

Symbols

d_b and D Bubble diameter (m)

D_T Column diameter (m)

f External forces $(\frac{N}{m^3})$

g Gravitational acceleration $(\frac{m}{s^2})$

G Gravitational force $(\frac{N}{m^3})$

I Identity matrix

p Pressure (Pa)

R Bubble radius (m)

S Surface tension force $(\frac{N}{m^3})$

t Time (s)

U Velocity field $(\frac{m}{s})$

V_T Rise velocity $(\frac{m}{s})$

w Atmosphere height (m)

ρ Density of cell $(\frac{kg}{m^3})$

ρ_o Density of continuous phase $(\frac{kg}{m^3})$

ρ_r Density ratio

ρ_g Density of gas $(\frac{kg}{m^3})$

ρ_l Density of liquid $(\frac{kg}{m^3})$

$\boldsymbol{\sigma}$ Stress tensor $(\frac{N}{m^2})$

μ Dynamic or absolute viscosity of cell $(\frac{Ns}{m^2})$

μ_o Dynamic or absolute viscosity of continuous phase $(\frac{Ns}{m^2})$

μ_r Viscosity ratio

μ_g Dynamic or absolute viscosity of gas ($\frac{Ns}{m^2}$)

μ_l Dynamic or absolute viscosity of liquid ($\frac{Ns}{m^2}$)

ν_g Kinematic viscosity of gas ($\frac{m^2}{s}$)

ν_l Kinematic viscosity of liquid ($\frac{m^2}{s}$)

γ Surface tension ($\frac{N}{m}$)

α Water volume fraction ($\frac{N}{m}$)

Operators

∇ Gradient

$\nabla\bullet$ Divergence

Δ Laplace Operator

$\frac{\partial}{\partial t}$ Partial derivative

$\frac{d}{dt}$ Total derivative

tr($\mathbf{A}$) Trace of A

$(\mathbf{A})^T$ Transpose of A

Abbreviations

BC Boundary condition

CFD Computational fluid dynamics

CV Continuous variable

DNS Direct numerical simulations

Eo Eötvos number

Fr Froude number

Ga Galilei number

M-CFD Multiphase computational fluid dynamics

MULES Multidimensional Universal Limiter with explicit solution

PISO Pressure implicit with splitting of operators

PLIC Piecewise linear interface calculation

Re Reynolds number

VOF Volume-of-fluid

We Weber number

1 Introduction

Multiphase flows are presented in a vastly natural and industrial processes of many different rates. Regarding the first ones they are in the rain, snow, fog, avalanches, mud slides, sediment transport, debris flows, groundwater, sand storms, volcanic eruptions, and countless other phenomena of our environment [11]. About the industrial processes the amount may be even larger than natural ones due to, virtually every processing technology must deal with multiphase flow; from the cavitation in turbinese and pumps to papermaking among many other. But also, they are presented in ourselves from blood flow to semen, as well as in biological and medical areas (from the bends to lithotripsy to laser surgery cavitation). It is impossible to create an adequate list that illustrates the diversity and ubiquity, therefore there is an unavoidable need in focusing in a specific field.

Centering the attention to gas liquid two phase flow in the industry, once again there are multiple applications. In the chemical industry, multiphase reactors as bubble columns are used to perform chemical reactions as polymerization, chlorination, hydrogenation or alkylation. In the nuclear context, Boiling Water Reactors (BWR) or Pressurized Water Reactors (PWR). Also in wastewater treatment plants, air-water or oxygen-water are used at different stages combined with microorganism to decrease the organic content of the sewage. Inclusive in one of the most important industries nowadays, the oil or petroleum industry is also an example of presence of two-phase flow as it exists in transport pipelines, pumps and production wells. Furthermore, they are presented in a huge range of general devices where the main energy exchanged is the heat, for instance boilers, condensers, phase separators, heat exchangers, etc. Following on from this in nuclear power plants, BWR and PWR under accident conditions, contain a steam-water mixture produced by the heat given by the fuel elements [12].

In all of these processes and activities, it is quite often important to be able to predict the flow behavior, then the efficiency and the productivity can be enchanced. Moreover, the safety of the plant design and its activity can be easily improved if the flow behavior is known. For example, an accident in a nuclear power reactor as it is said above. Nonetheless, the understanding of two-phase flow in terms on interfacial behavior, dynamics and heat exchange is far from the level of the single-phase flow knowledge. The best way to study this flow is combining theoretical and computational models to use these models to larger scale facilities than the experiments used for validation, since the experimental applications are limited by the size of the laboratory and by the complex geometries. In addition, the measurement devices are expensive and not as exact as it would like. As a result of that Computational Fluid Dynamics softwares are taking more importance in these days. There are free and commercial CFD softwares as in mostly of softwares, but in this field the development of both are quite similar, these days. Lot of literature supported this idea, that commercial and open-source CFD softwares are in the same level, as it can be proved in [13] and [14] among many others. The software

OpenFOAM was chosen to run every simulation under the present thesis. The main reason to choose an open-source code was because it can be seen with what equations is working and how it solves them. According to that it is easier to understand the phenomena that is simulated and the equations which governs it. Another reason, which may be has less importance, is for saving money since it works as commercial ones.

Broadly speaking, the objective of this thesis is to check that for the studied cases, an initially spherical bubble starting from rest in quiescent water in 2 and 3 dimensions; OpenFOAM with the algorithm IsoAdvector, provides proper result with respect to the experimental and numerical ones, also that these results are similar to other software ones, specially commercial softwares. Specifically, it is wanted to set a grid size which ensures a well balance between time execution and accuracy, to obtain three characteristics that define the dynamic of a single bubble: rise velocity, trajectory and shape. In detail the main objectives of this thesis are as follows:

- Present a literature survey on experimental, numerical and computational analysis of the trajectory, bubble shape and rise velocity of an initially spherical bubble starting from rest in quiescent water.
- Test differences between the algorithm IsoAdvector (InterFlow) and MULES (InterFoam).
- Repeat the 2D simulations of Krishna et al. (1999) [8] with IsoAdvector and compare them with the simulations results and experimental data base shown in the named article.
- Compare the 2D rise velocity with the equation develop by Collins (1965) [15].
- Set 3D simulations based on the experimental data shown in Krishna et al. (1999) [8].
- Compare 3D rise velocity with experimental data shown by Krishna et al. (1999) [8] and Haberman et al. (1953) [16].
- Compare 2D and 3D bubble shapes and trajectories with the simulations done by Kumar Tripathi et al. (2015) [5].
- Compare the 3D rise velocities with the equation proposed by Jamialahmadi et al. (1994) [9].
- Present a few comparisons between real images and simulation images.

2 Theory

2.1 Multiphase flows

In the present thesis, the terminology multiphase flows refer to any fluid flow consisting of more than one phase or component. However, it is excluded those cases in which the substances are well merged above the molecular level. Generally, multiphase flows can be separated in two topologies: disperse flows and separated flows. The first ones are compound by a disperse phase (bubbles or drops) distributed in a connected volume of the continuous phase (water in this thesis). The latter flows are formed by different fluids separated by interfaces, it could be said that there are two continuous phases. There are three methods in which multiphase flows are investigated: experimentally (laboratory tests), theoretically (mathematical equations) and computationally. Of course that there are some experiments in which the last prototype is tested, however that is unusual. Experimental studied have been found to provide useful results only for limited cases with restricted complexities of the multiphase flow. Besides, in many cases , the model tested has a different scale than the prototype, and the prototype behavior is estimated based on the experimental tested but using mathematical equations or computationally.

Thus, the understanding of multiphase flows should rely on theoretical and computational models which implicates a bigger barrier, in terms of knowledge, than the one with experiments. Nowadays it may be possible to code the Navier-Stokes equations and computing with a huge detail the multiphase flows. Although, much still remains to be done, the Computational Fluids Dynamics (CFD) are working quite well and are being validated with lot of experiments. Despite of the low complexity of the experimental data obtained, which match with the computer simulations, this is only the base to ensure that CFD works proper. In addition, it should be taken into consideration that CFD and mathematical models work hand in hand since CFD are able to solve with a huge exactitude the equations that describe the real phenomena.

In the present thesis the covered multiphase flows are disperse, where there are mainly two type of models, trajectory models and two-fluid models. In trajectory models, the movement of the disperse phase is analyzed by following the movement of the actual particles or the movement of the representative particles. The features, primarily the trajectory, of the flow that surround the particles are derived on the drag, lift and moment forces (thermal equations may also be tracked). Concerning the two-fluid models, which will be simulated under this thesis, the disperse phase is treated as a second continuous phase intermingled and interacting with the continuous phase. Effective conservation equations (of mass, momentum and energy) are developed for the two fluid flows; these included interaction terms modeling the exchange of mass, momentum and energy between the two flows. As a result of that, these models omit the discrete nature of the disperse phase and estimate its effects upon the continuous phase, having to implement averaging processes to calculate the properties of the

disperse phase, which implicates notable issues. Despite of this, in theory, one can solve the single phase fluid flow equations in the two streams, coupling them through appropriate kinematic and dynamic conditions at the interface. There are some examples of this in the literature [17], [18], [19] and [20].

A flow pattern or flow regime is a singular kind of geometric distribution of the substances. They are often identified by visual inspection, though other methods like analyzing some variables as the fluctuations in the volume fraction have been used [21]. For some simple geometries such as vertical and horizontal tubes, a great amount of researchers have been conducted to set the dependence of the flow regime on volume fraction, on volume fluxes, on fluid properties as viscosity, surface tension and density and on air velocity with column diameter. However, the flow regime maps apply only to specific pipe size and fluids. Additionally, even for these particular maps the boundaries between different zones are not clear, so there are transitions zones which are not so much precise, see Figure 1. Notwithstanding the great amount of investigations done there is not still a dimensionless flow pattern map which incorporates the whole parametric dependence of the boundaries on the fluid characteristics. Here, it is only going to briefly describe the flow pattern of a vertical tubes, due to the simulations done are in vertical tubes.

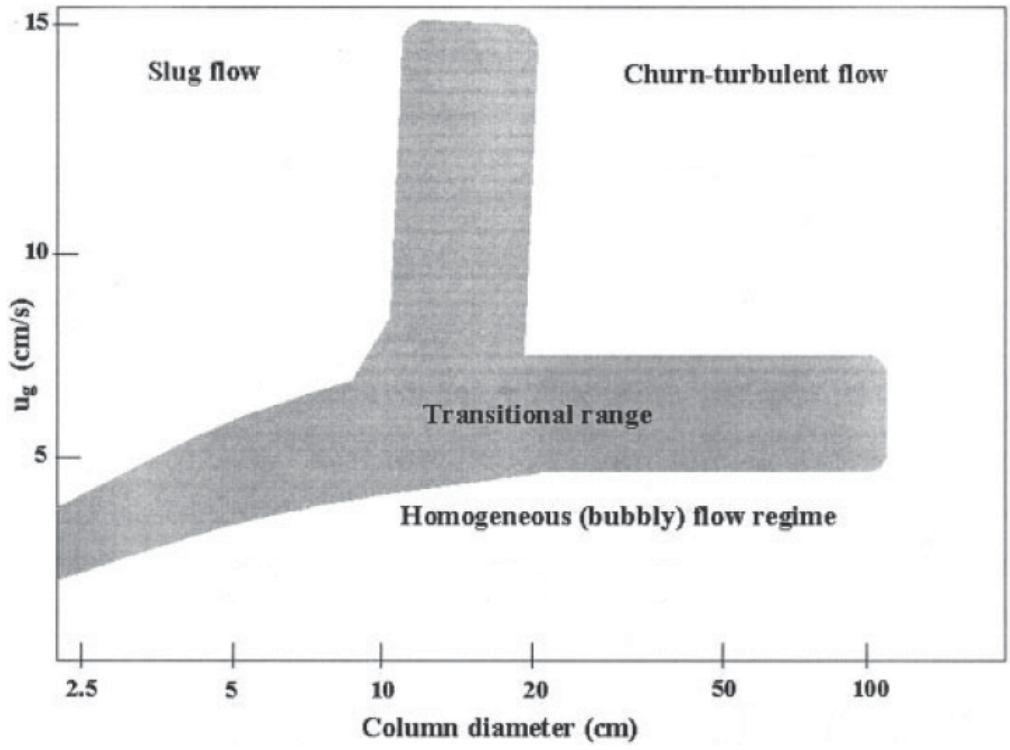

Figure 1: Flow-regime map. Source: [1]

Figures 1 and 2 show the flow regime maps and the representation of how they look like. Generally, they may be described through two concepts: disperse term and separated term. The first term refers to that multiphase flows where the disperse

phase is extensively distributed as particles (drops or bubbles) in the continuous phase. On the other hand, the latter term consists on parallel flows formed by two or more phases. The asymptotic limit of a disperse flow in which the disperse phase is distributed as an infinite number of infinitesimally small particles, bubbles, or drops is termed like homogeneous multiphase flow. In this kind of flow the motion between both phases may be zero, then they are called homogeneous flows, although there are many practical disperse flows, in which the particles are much smaller than the pipe diameter and the relative motion is significant, they are called bubbly flows. To summarize: one of the basic characteristics of a flow pattern is the degree of separation of the phases into streamtubes of different concentrations. The degree of separation will, in turn, be determined by (a) some balance between the fluid mechanical processes enhancing dispersion and those causing segregation, or (b) the initial conditions or mechanism of generation of the multiphase flow, or (c) some mix of both effects [11]. The second basic characteristic is the level of intermittency in the volume fraction, defined as the degree of periodic separation in the streamwise direction, for instance the slug or churn flows in vertical columns (see 2. This last feature is the result of instabilities, in which the kinematic waves grow in an opposed way of nominally steady flow to cause significant separation of the phases.

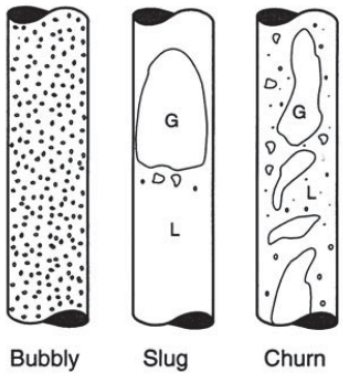

Figure 2: Sketches of flow regimes for two-phase flow in a vertical pipe. G and L refer to gas and liquid phases respectively. Source: [1]

2.2 Bubble generation

Before starting with the bubble generation it is essential to define what is a bubble: simplifying, it is a thin sphere of liquid enclosing another gas. Under this thesis, the word gas always refers to air. Evidently, there are an immensely different methods to generate bubbles. Here, it will be focused on those that are useful to generate a single bubble, in concordance with the simulations computed. Under this field, there are from the easiest ones to the most complicated ones. One of the simplest consists of an air injector, which has a valve to regulate the air flow, in a water container, so depending of the grade of opening of the valve it will be created one or multiple bubbles. This system, for instance was used in [2]. On the other hand, one of the most complicated system is the laser-induced breakdown in water, which is an important issue in the field of laser medical care. With this system it can be generated micro bubbles (from several tens of micrometers to several hundreds of nanometers). Like in the simplest method, this one is able to produce a single bubble or a bubbly flow in function of the laser pulse energy. The reader can found more information in [22]. The last bubble generation process that will be briefly explicated is the called gentle-push method [23]. The complexity of this method is located in an intermediate level, between the two referred to above. The importance of this system is that it can be generated a single bubble in a quasi-static state. As a result of that it is a good experimental method to compare with a simulation of a single bubble rising which the initial condition is a null velocity field. In fact, there is an article in which that comparison is done [24].

With respect to theoretical methods about how a bubble is generated there are two principal models: the one proposed by Kumar et al. (1969) [25] and the one proposed after by Gaddis and Vogelpohl in 1986 [26]. The two models explained the bubble formation under the state of constant flow conditions. Concerning the first model, it is based on three phases: the expansion of the bubble, which remains the contact with the nozzle. The second corresponds to the phase when the bubble moves away from the nozzle, remaining the contact with the nozzle through a neck. Finally the bubble left the nozzle, which would be the total separation phase. In Figures 3 and 4 all the phases are skectched and photographed. The volume of the single bubble can be calculated as the sum of the volume of each phase, the reader can see the methodology to calculate the final volume in [25]. Here, it will be explained only the influence of each variable in this final volume, but none equation will be shown.

The surface tension has a influence in the volume of the bubble in function of the flow rate and the viscosity:

- If the flow rate is close to zero then the volume of the bubble depends only on the surface tension and the buoyancy forces, being the first one in the numerator and the second in the denominator.

- For low viscosity liquids the influence of the surface tension decreases continually

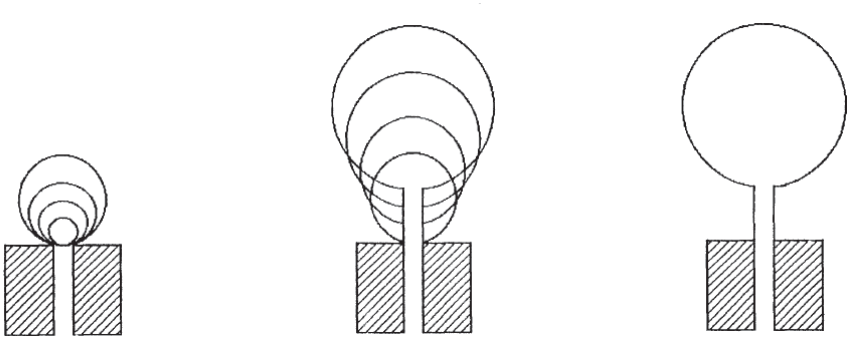

(a) First phase. (b) Second phase. (c) Third phase.

Figure 3: Bubble formation phases. Source: [2]

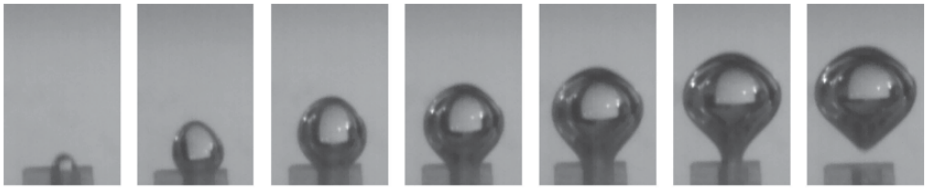

Figure 4: Series of instantaneous states of bubble formation in the experimental liquids. Source: [3]

when the flow rate is increased. Up to a value, in which the volume of the bubble is constant regardless the increment of the flow rate.

- From the opposite position for high viscosity liquids the effect of the surface tension has a little impact. The value of the flow rate for which the surface tension can be neglected is smaller than in the other cases.
- When the diameter of the nozzle is small the surface tension has a low influence.

The viscosity (viscosity of the liquid) effects are:

- An increase in viscosity increases the bubble size. Nonetheless, it can be despised for low flow rates.
- Its effect is considerable for high flow rates.
- It is also remarkable when the diameter of the nozzle and the surface tension are small.

The density sometimes have a noticeable effect in the volume of the bubble and others has not:

- If the viscosity and the flow rate are little then the bubble volume decreases when the density is increased.

- When the value of flow rate is high and the viscosity and the diameter of the nozzle are small the density effect can be neglected.
- When the viscosity is quite big and the nozzle diameter is small then the bubble volume decreases when the density is increased.

Concerning the model proposed by Gaddis and Vogelpohl in 1986 [26], this predicted the bubble diameter when the bubble leaves out the nozzle but it is still in contact whith this trough a neck, whereby it corresponds with the second pahse of the method proposed by Kumar et al. (1969) [25]. The new contribution is the pressure force included in the method and the explanation about the expansion of the bubble even when the neck connector is presented. As in the method already explained it will not be shown any equation due to its application is out of the thesis scope. In Figure 5 it can be seen all the volumetric and surface forces and their directions presented in the phase named. The volumetric ones are the forces due to: buoyancy (F_b), pressure (F_p) and the inlet gas movement (F_m). The surface forces that are the opposing forces to the volumetric ones are: surface tension (F_s), drag (F_d) and inertial (F_i) forces.

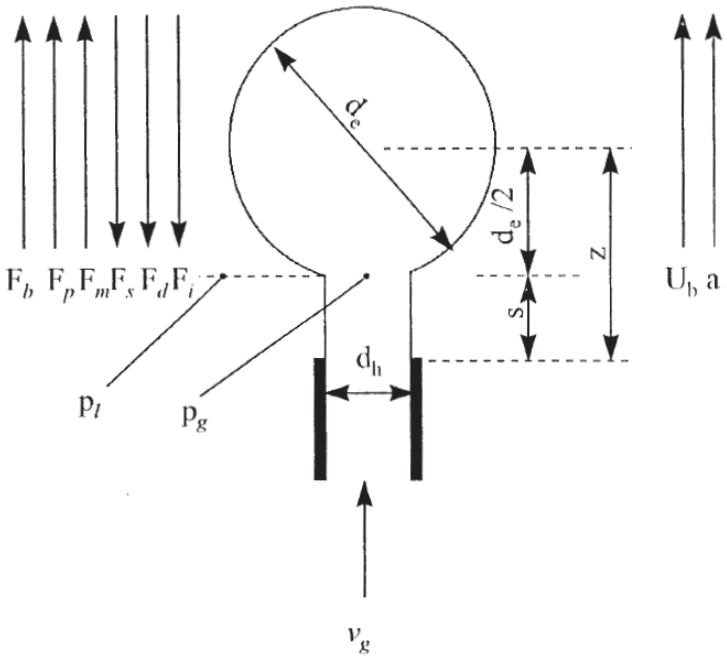

Figure 5: Geometric model of a spherical bubble held to the nozzle through a cylindrical neck. Source: [2]

2.3 Bubble dynamics

In this section the bubble dynamics will be described according to the shape, trajectory and rise velocity. The kind of trajectory and shape are associated between them, consequently they will be explained together. Afterwards, rise velocity theme will be developed. The bubble movement is complex when it is not a straight line, and it can be described as a combination of two kind of moves: vibrations of a rigid body with deformations of a non-rigid body [2]. There are two main options to describe trajectories and shapes: non dimensional numbers and equations. Firstly, the influence of dimensionless numbers will be explicated. Secondly, the equation that characterize the dynamic of spherical bubbles. The non dimensional numbers used to predict the shape and the path are:

- Reynolds number (Re): ratio of inertial forces to viscous forces.

$$R_e = \frac{\rho_o U L}{\mu_o}$$

- Weber number (We): it compares the inertia of the fluid with its surface tension.

$$W_e = \frac{\rho_o U^2 L}{\sigma}$$

- Eötvos number (Eo): ratio of the gravitational force to the surface tension.

$$E_o = \frac{\Delta\rho g R^2}{\sigma}$$

- Galilei number (Ga): ratio of the gravitational force to the viscous force.

$$G_a = \frac{\rho_o \sqrt{gR} R}{\mu_o}$$

- Morton number (Mo): ratio of gravitational and viscous force to the surface tension.

$$M_o = \frac{E_o^3}{G_a^4}$$

There are some articles where the shape of the bubble is predicted based only on We, see [27] and [28]. There are also others where the shape and the trajectory are prognosticated in function of Re, for instance in the report [29]. Besides, some literature set the bubble's path and the transitions area according to both dimensionless number (We and Re), see the Ph.D. thesis [30]. The problem of that predictions is that the terminal velocity have to be known to calculate the numbers needed. That

is an issue due to the velocity is not usually known a priori. As a result of that and for this thesis, it is more useful to use Eo, Ga and Mo numbers, since one of the objectives of the present thesis is to calculate the terminal velocity.

Regarding the Mo number, if its value is high then the gravitational and viscous forces prevail and the way of the bubble is typically an straight line [31]. The reason of that is because the bubble is usually spherical (or it is near the spherical edge) or the Reynolds number is low, which can be checked in Figure 6. Nevertheless, the graph desired should not plot any number related to the bubble velocity.

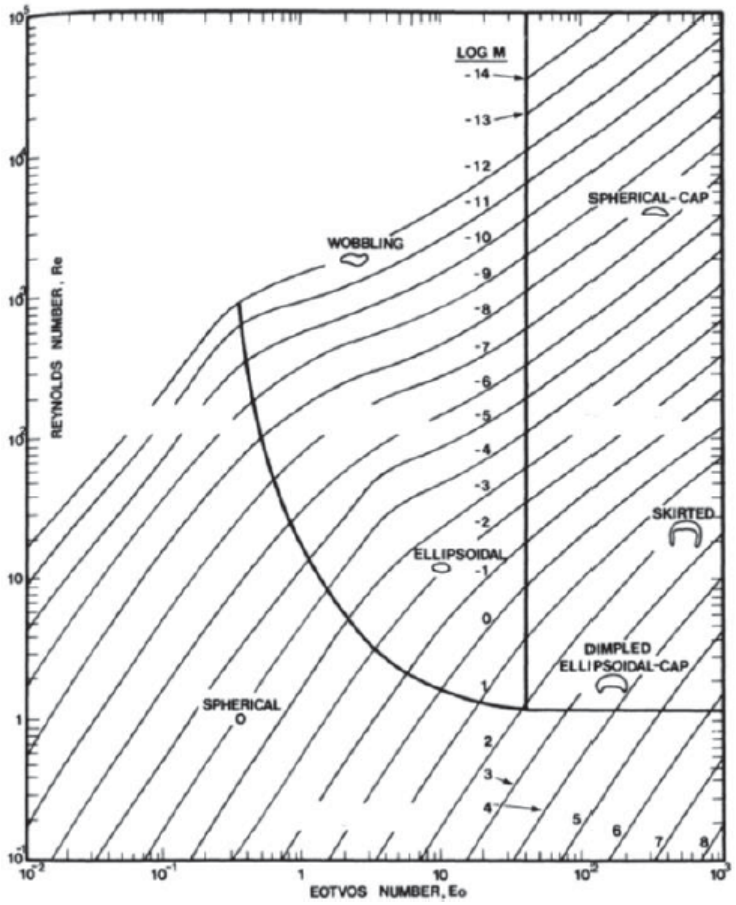

Figure 6: Bubble shape in function of Eo, Re and Mo numbers. Source: [4]

About the values of Eo and Ga number, where the bubble velocity is not presented, there have been set some regions, in which the bubble trajectories and its shapes are fixed. As it can be seen in Figure 7 there are five different regions [5]:

- I: corresponds to low Eötvös and Galilei numbers. In this domain, the value of the surface tension is big due to the low Eo number and the effect of the gravitational force is low because of the value of both numbers are little. For all that it is reasonable that the bubble preserves its integrity. The bubble accomplishes an ellipsoidal shape, which is constant on time. Besides, it takes a terminal velocity going straight upwards (vertical line). In this region, the

bubble is axisymmetric.

- II: this region contains high Eötvös numbers and low Galilei ones. The bubble here has two distinct features, an axisymmetric cap with a thin skirt trailing the main body of bubble. The bubble, generally, travels in a vertical line as in the region number one, however, in the beginning the path can be different. Similarly to the beginning, near to the skirt region the bubble shape changes, nevertheless, that change is not included in the thesis scope.

- III: region III refers to low Eötvös number and high Galilei number. For this reason the surface tension force has to be taken into account such as the inertial force. Here, the bubble does not travel in a vertical line, it goes up in a spiral manner or a zigzag. The bubble does not break up, although, its shape change with time.

- IV: This narrow region covers a medium value of the product Galilei-Eötvös number. Consequently, there are two possible cases as it can be seen in Figure 7: high Eötvos number with medium-low Galilei number and the opposite one (low-medium Eötvos with high Galilei numbers). In the first sample the bubble breaks into a big axisymmetric spherical cap and a lot of small capsule bubbles in the trail of the cap. It called peripheral breakup [5]. In the second case, in the beginning a new breakup behavior is observed, however, so far it has not been possible to define a consolidated dynamic. But, on the other hand, it has been proved that the bubble reach a constant shape and a terminal velocity.

- V: Region number five comprehends high Eötvos and Galilei numbers. Accordingly, in this domain the bubbles are under the effect of low surface tension force (high Eötvos number) and high inertial forces (high Galilei number). The shape in this region is common (although it is not constant): a dimple formation in the bottom centre leads to a change of topology to a doughnut-like or toroidal shape as seen in the region V of Figure 7. Near to the border with the region IV, in addition to the change of topology, the bubble breakups in a small satellite bubbles. The bubble shape changes as Galilei and Eötvös numbers are increased further, on account of that, the shape is not permanent like in the other regions.

With respect to the equations that govern the bubble dynamics the Rayleigh-Plesset equation has been chosen in view of the concordance with the scope of the present thesis. This equation rules the dynamics of spherical bubbles in an incompressible fluid [32], which is water under this thesis. Each term of the equation is defined in Section Symbols and Abbreviations . As it will be seen in Section 3.3 OpenFOAM works with the Navier-Stokes equations, what includes this equation, due to it is derived from the Navier-Stokes equations (assuming spherical symmetry). Therefore this is only an example of how to calculate the radius of an initial spherical bubble as a function of time as the outside (or inside pressure) is known. The equation is presented below.

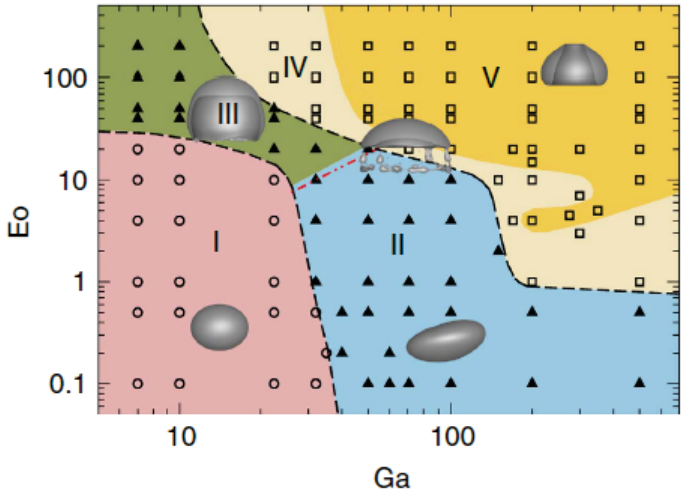

Figure 7: Different regimes of bubble shape and behavior. The circles represent axisymmetric bubbles, the solid triangles asymmetric ones and the squares breakup regions. Source: [5]

$$R\frac{d^2R}{dt^2} + \frac{3}{2}\left(\frac{dR}{dt}\right)^2 + \frac{4\nu_l}{R}\frac{dR}{dt} + \frac{2\sigma}{\rho_l R} + \frac{\Delta P(t)}{\rho_l} = 0$$

Finally it is briefly explained the different methods to obtain the rise velocity and it will be justified the choice of one of them. There are three main approaches to calculate the terminal velocity [33], which are based on: balance of forces, dimensionless numbers or wave analogy. About the first one the main issue is that the drag coefficient has to be calculated, and it is usually a function of Re number (the terminal velocity). With the dimensionless number there a lot of equations that depending on the bubble shape, for instance in each article it has been set an specific equation for each bubble shape [34], [35], [36], [37] and [15]. The problem here is that the range of dimensionless is quite short. As a result of that the wave analogy seems to be the right method.

What it was looking for was an equation that could be applied for a vastly range of non dimensional numbers, in other words, for a great number of bubble diameters even the bubble shape is changed. That equation, it would be better to say set of equations, was found, and it is based on a wave analogy approach, combining the cases when the viscous effects are significant with those cases when the surface tension effects are still important:

In 1963, Moore [38] presented Equations 1 and 2 for the rise velocity when the viscous effects are significant:

$$V_{T1} = V_{Tpot}(1 + 0.73667\frac{\sqrt{gd_b}}{V_{Tpot}})^{1/2} \tag{1}$$

$$V_{Tpot} = \frac{1}{36}\frac{\Delta\rho g {d_b}^2}{\mu_l} \tag{2}$$

In 1976, Lehrer [39] proposed Equation 3 for the rise velocity when the surface tension effect are important:

$$V_{T2} = (\frac{3\sigma}{\rho_l d_b} + \frac{g d_b \Delta\rho}{2\rho_l})^{1/2} \tag{3}$$

Finally, in 19994 Jamialahmadi et al. [9] united those equations based on a wave analogy approach obtaining:

$$V_T = \frac{1}{\sqrt{\frac{1}{V_{T1}^2} + \frac{1}{V_{T2}^2}}} \tag{4}$$

The set of Equations formed by from 1 to 4 is compared with a great amount of experiments in Figure 4. As it can be seen the set of equations match quite well with the experiments in distilled water. Moreover, the simulations that have been run under the present thesis are included in the range of values that this set covers.

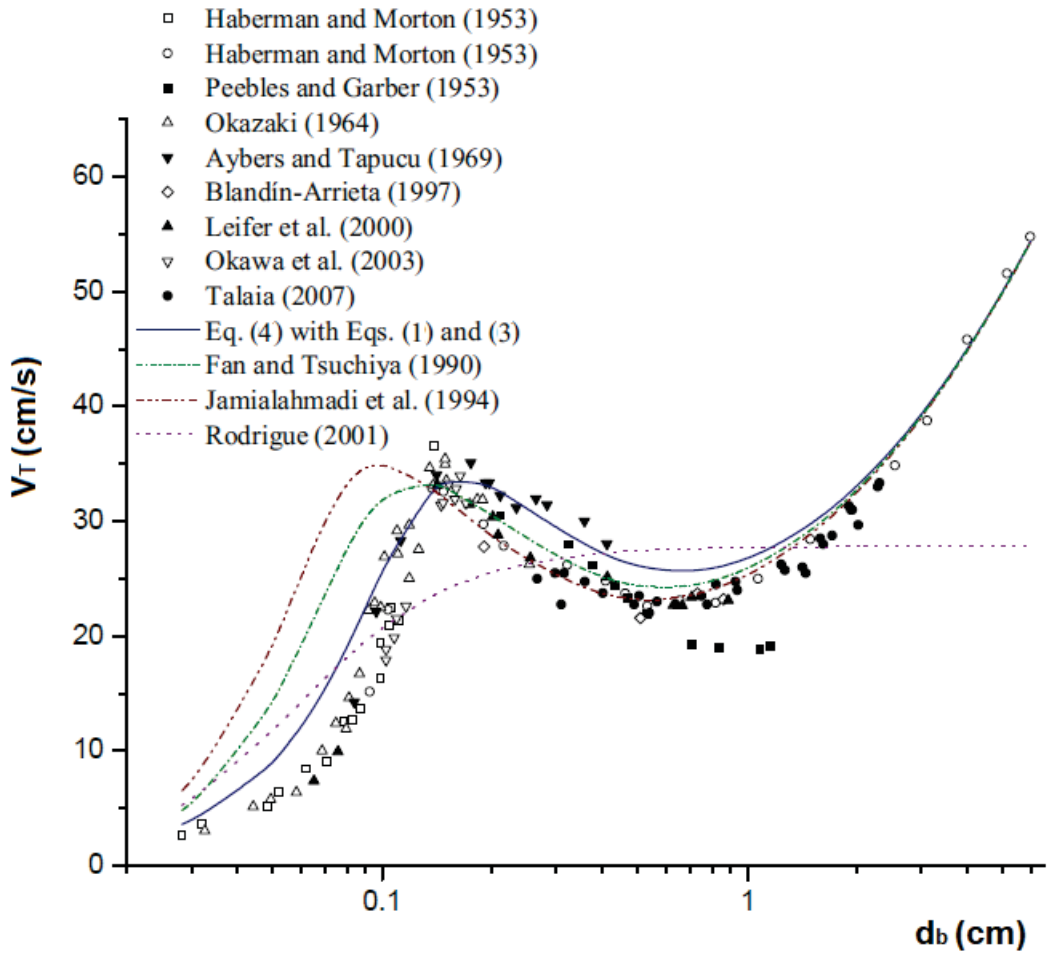

Figure 8: Comparison between predictions of equations and experimental data for bubble terminal velocity through distilled water ($7.4 < \mathrm{Re} < 32500$; $0.002 < \mathrm{We} < 245$; $0.01 < \mathrm{Eo} < 475$) at 20-28 °C. Markers correspond to experimental data, and lines to predictions from the equations. Source: [6]

.

3 Governing equations

In the next section it shown the main governing equations of the solvers that were used to run the cases. These solvers are well defined in Section 3.2 and the simulations in Section 4, however, here it is needed to appoint some characteristics of the studied cases. In the investigated cases the species are water and air, consequently they are immiscible. The cases can be considered isothermal and the compressibility effects can be neglected because of the low velocities of the air [40]. Ergo the fluids studied can be treated as Newtonian fluids.

3.1 Navier-Stokes equations

The main governing equation is the Navier-Stokes momentum equation, which defines the motion of Newtonian fluid. The easiest definition of Newtonian fluid could be: Those fluids that their viscosity remains constant for a constant temperature (no matter the amount of shear applied). These fluids have a linear relationship between viscosity and shear stress.

The Navier-Stokes momentum equation can be written in the conservation form of the equations of continuum motion:

$$\frac{\partial \rho \mathbf{U}}{\partial t} + \nabla \bullet (\rho \mathbf{U}\mathbf{U}) = \nabla \bullet \boldsymbol{\sigma} + \mathbf{f} \tag{5}$$

Where ρ is the density of the current cell, $\mathbf{U}$ is the velocity field, σ the stress tensor and $\mathbf{f}$ the external forces. The stress tensor σ can be expressed as:

$$\boldsymbol{\sigma} = -p\mathbf{I} - \frac{2}{3}\mu(\nabla \bullet \mathbf{U})\mathbf{I} + \mu\nabla\mathbf{U} + \mu(\nabla\mathbf{U})^T \tag{6}$$

Where μ is the absolute or dynamic viscosity and $\mathbf{I}$ the identity matrix. Combining Equations 5 and 6 one obtains:

$$\frac{\partial \rho \mathbf{U}}{\partial t} + \nabla \bullet (\rho \mathbf{U}\mathbf{U}) = \nabla \bullet \left[-p\mathbf{I} - \frac{2}{3}\mu(\nabla \bullet \mathbf{U})\mathbf{I} + \mu\nabla\mathbf{U} + \mu(\nabla\mathbf{U})^T\right] + \mathbf{f} \tag{7}$$

Finally it may be modified last Equation 7 developing the last bracket, applying the divergence in each term, then the pressure term is the pressure gradient, $(\nabla \bullet (-p\mathbf{I}) = -\nabla p)$ and knowing that $\nabla \bullet \mathbf{U} = \mathrm{tr}(\nabla\mathbf{U}) = \mathrm{tr}(\nabla\mathbf{U})^T$, one obtains:

$$\frac{\partial \rho \mathbf{U}}{\partial t} + \nabla \bullet (\rho \mathbf{U}\mathbf{U}) = -\nabla p + \rho\nu\Delta\mathbf{U} + \nabla \bullet \left(\rho\nu\left[(\nabla\mathbf{U})^T - \frac{2}{3}\mathrm{tr}(\nabla\mathbf{U})^T\mathbf{I}\right]\right) + \mathbf{f} \tag{8}$$

Where in the cases studied in this thesis $\mathbf{f}$ refers to the gravity force ($\mathbf{G} = \rho\mathbf{g}$) and the force associated to the surface tension effects for a single bubble ($\mathbf{S} = \nabla(\frac{2\sigma}{R})$, where σ is the surface tension, R the bubble radius and the gradient is need to be in concordance with the units. Hence $\mathbf{f} = \mathbf{G} + \mathbf{S}$. The Navier-Stokes equation is shown in this form (8) to facilitate the comprehension of the OpenFOAM code, as will be seen further on Section 3.3. As it is said above the compressibility effects can be neglected because of the low velocities of the air, therefore the densities are considered constant which leads to the velocity field being divergence free everywhere. To this last equation should be added: firstly the continuity equation, since fluids are incompressible:

$$\nabla \bullet \mathbf{U} = 0 \tag{9}$$

Secondly, three equations that defined the local fluid properties (10 and 11), which are density and dynamic viscosity, and the variation of the water volume fraction (α) with time and position (12), which is called transport equation.

$$\rho = \alpha\rho_l + (1 - \alpha)\rho_g \tag{10}$$

$$\mu = \alpha\mu_l + (1 - \alpha)\mu_g \tag{11}$$

$$\frac{\partial\alpha}{\partial t} + \nabla \bullet (\alpha\mathbf{U}) = 0 \tag{12}$$

The last term of Equation 12 should be $-\nabla \bullet (\alpha(1 - \alpha)\mathbf{U}_r)$, however it is ignored because is a compression term. Additionally, the solver algorithm most used in the simulations done (IsoAdvector) does not use such term. At the end, the system that the software is going to solve is formed by Equations: 8 - 12.

3.2 VOF methods

All the simulations presented in this work were carried out using the volume of fluid (VOF) method, which was developed by Hirt and Nichols [41] starting a new trend in multiphase flow simulation. The conventional VOF method is based on indicator functions. An indicator function allows us to know the volume fraction of one phase (water under this work), in other words, it indicates whether the cell is occupied by one fluid or another, or a mix of both. The momentum, continuity and transport equations, Equations 8, 9 and 12 respectively, are solver simultaneously for an indicator function. The water volume fraction can take values within the range $0 \leq \alpha \leq 1$, where the limits correspond to regions with only one phase ($\alpha = 0$ for gas and $\alpha = 1$ for water). Cells with water volume fraction values between zero and one contain a free surface. In accordance to this gradients of the water volume fraction are applied in the interface regions [42]. Ergo, the effective fluid throughout each cell is formed by a mix of both immiscible fluids. The physical properties of the effective fluid are calculated as weighted averages in function of the distribution of the water volume fraction, hence they only vary across the interface. These properties are defined by Equations 10 and 11.

On the one hand the critical issue of VOF methods is the conservation of the phase fraction in the free surfaces. This problem is notable in those cases where the density ratio is high, then small errors in volume fraction may provoke considerable errors in calculations of physical properties. Besides, to determinate an appropriate surface curvature, which is necessary to compute the surface tension and pressure gradient across a free surface, is fundamental the proper calculate of the phase fraction distribution. It is not an easy labor to guarantee boundedness and conservativeness of the phase fraction. Various attempts have been made in order to overcome these difficulties [43], [44], [45], [46] and [47].

On the other hand one of the main advantages that offers this method is the time reduction introduced with regard to solve the whole domain. In addition, the error imported also may be enough small to have no effect in the solution. Accordingly to a great amount of open literature the VOF technique provides proper results, which have been successfully compared with experimental and numerical data. For instance, numerical analyses of a two-dimensional single bubble in a stagnant liquid and in a linear shear flow were conducted in [48] using the VOF method. The results obtained support that VOF method gives qualitatively appropriate predictions for the effects of the Mo and Eo numbers. Furthermore, VOF technique has been proved to be a good method for providing an accurate description of the bubble rise velocity. It can be seen in the article [49].

In view of all that has been set out above, it is considered that it should be chosen the proper VOF method to analyze bubbly flows, since there are a lot of branches of this method. For further information, the reader is able to go quite deep into the VOF methods with the information available in these two books: from Versteeg

and Malalasekera [50] and Ferziger and Peric [51]. In addition, there is a thesis [52], in which it is described with considerable detail how this method is applied in the OpenFOAM's frame.

3.2.1 InterFoam

First of all a brief definition about interFoam: it is a solver for 2 incompressible, isothermal immiscible fluids using a VOF phase-fraction based interface capturing approach. Accordingly, this solver match with our simulation requirements. However, it should be highlighted that interFoam applies the OpenFOAM specific algebraic VOF scheme called MULES (Multidimensional Universal Limiter with Explicit Solution) for the task of advecting the sharp interface [53]. That it should be noted because of the MULES scheme has a number of desirable properties [54]:

- It preserves the volume of fluid, i.e. it does not artificially create or destroy fluid.
- It keeps the so-called volume fraction field in the physically meaningful range between 0 and 1.
- The interface stays sharp to within a few cell widths.
- It works on unstructured meshes both in 2D and 3D,
- It is efficient so only a minor fraction of the calculation time is spent on interface advection.

Nevertheless, in Section 3.2.2 there are some times that MULES may be rather inaccurate in its solution of the interface advection problem. The reader may found an exhaustive description of the MULES method in Chapters 2 and 5 of the PhD. thesis of Santiago Márquez Damián (2013) [55]. Firstly it is going to be described the folders and directories that regularly compound any case similar to the simulation ones in this thesis. Secondly the solution procedure used in the solver will be explained to solve the governing equations.

The cases run with the solver interFoam may generally be structured as is shown in Figure 9. Every case is saved as a directory, which must contain at the minimum three folders: /0/, /system/ and /constant/. The /0/ directory contains all the initial flow fields relevant for the solver. As it can be seen in Figure 9, the folder is formed by the velocity field (/U/), the water volume fraction (/alpha.water/) and the pressure (/p_rgh/), which is defined as the total pressure minus the hydrostatic one ($p_{rgh} = p - \rho g h$). Here is where the boundary and the inlet conditions are fixed.

Solution controls, mesh generated, discretization schemes, air domains and time step controls are situated in /system/ folder. The solution controls are written in the

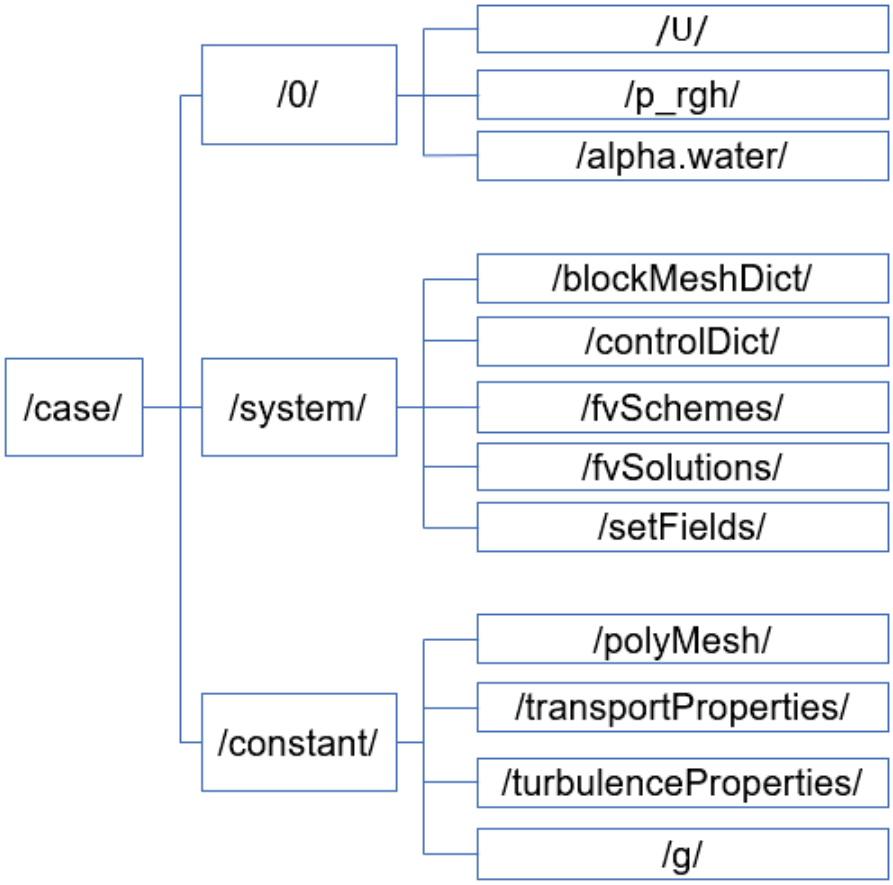

Figure 9: Boundary conditions of the case

file called /fvSolutions/, where things as the solution procedure, maximum number of iterations and maximum errors are fixed. In the /blockMeshDict/ file block-structured meshes can be generated in text file format. The file /fvSchemes/ contains the time and space discretization and the interpolation methods (the information exposed in 3.3). In /setFields/ directory can be found the air domains. The steps are to define the whole domain with water in the alpha.water file, from then the zones where there is air are set in this directory. The file /controlDict/ manages the simulation duration, the time steps and the print-out interval among many other things. Summarized it controls the simulation times and the output data.

In the constant directory you will find includes the mesh storage (folder /polyMesh/), the material properties (/transportProperties/), the turbulence properties (/turbulentProperties/) and the gravity force field (/g/). Regarding the present thesis the defined properties are the density and the viscosity of water and air, and the surface tension. The file /turbulentProperties/ includes the type of flow, which will be treated as laminar and Newtonian. While the case is running, new time dumps are written in their own directories, updating the data for the next time step.

Concerning the solver algorithm used to solve the types of problems under considera-

tion here, the PISO (Pressure Implicit with Splitting of Operators) loop was chosen. The main reason is that this algorithm works proper for transient calculations and for low Courant numbers (less than one) [56]. As it will be check, all the simulations run in the present thesis match with both approaches. The PISO approach was proposed by Issa (1986) [57]. It consists on three steps for each time step and the iterations are only needed for the two last steps. One summary of this algorithm is presented by [58].

- 1. Momentum predictor: The momentum equations are optionally solved using a best-guess pressure field to produce a best-guess velocity field. However, Issa (1986) [57] notes that while this "momentum predictor" step is formally required for the method, many applications do not require it, and can proceed straight to the second step using the previous time-step's velocity field.

- 2. Using the previous velocities the pressure field is obtained. Therefore, the first estimate of the new pressure field is obtained.

- 3. The velocity field is corrected using the new pressures.

Within each time step, additional equations for multi-phase flow are solved before the PISO algorithm, while other equations, such as turbulence models, are solved afterwards. To see with exactitude the sequence of the solution see section 2.5.3.4 of [59]. The reader can found further information about this algorithm in [60] and [53].

3.2.2 IsoAdvector

Due to the fact that interFoam with MULES does not seem to converge to the correct solution even for very simple test cases, as Figure 10 shows and as it will be seen in Section 4.2.2, a new VOF algorithm called IsoAdvector was developed. The novelty of the IsoAdvector concept consists of two parts [7]: First, the reconstruction step, where iso-surfaces in the subcell interface are utilized for this step. Second, from that surface, the time evolution within a time step of the submerged face area is obtained. Integrating this area over the time step provides a proper estimation of the total volume of the flow transported across the face.

For understanding better the last paragraph the Piecewise Linear Interface Calculation (PLIC) technique proposed by Youngs in 1982 [61] is described with a 2D example. Although IsoAdvector algorithm is different than PLIC technique, the do similar things, and both are geometric VOF. Nowadays a great amount of computer codes, as OpenFOAM, ANSYS fluent and STAR-CCM, used VOF with PLIC. The main objective of this method is to achieve an accurate interface reconstruction in a complex geometric domain. As it was said in Section 3.2 governing equations are discretized and the domain is divided into cells or control volumes. Once governing equations are solved, the velocity ($\mathbf{U}$) and volume fraction (γ) fields are stored at the center of each computational cell, which correspond to the blue points in Figure

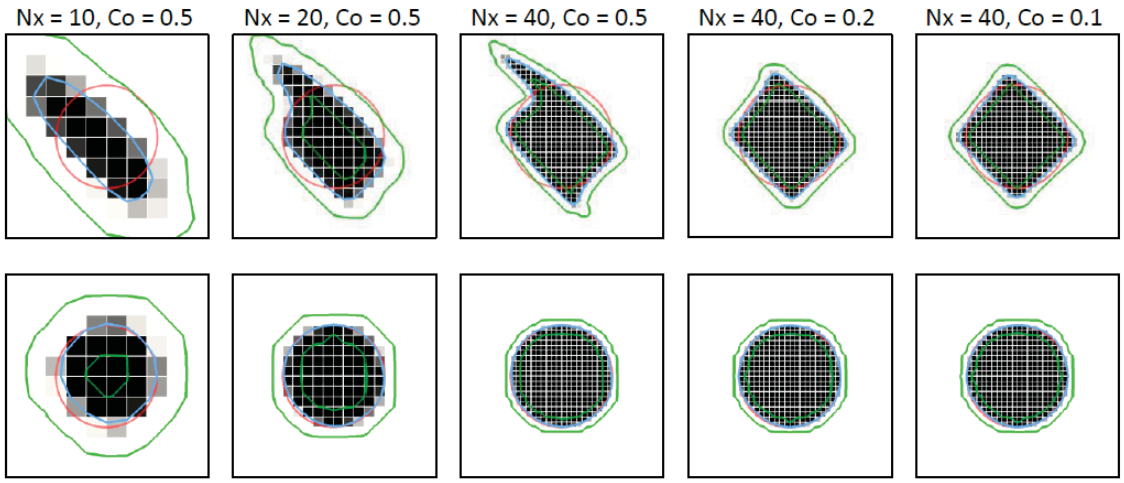

Figure 10: Shape of an initially circular volume of fluid after 4 seconds advection in a constant, uniform velocity field $U = (1, 0.5)$. The first row correspond to MULES and the second to IsoAdvector. Red circles are exact solution. Blue curve is VOF = 0.5 contour and green curves are VOF = 0.01 and 0.99 contours. Source: [7]

11; while **U** on the cell boundary or interface is calculated by interpolation. Then the interface reconstruction procedure to construct line segments in the interface cells starts. Firstly the normal direction of the line segments is calculated: In the PLIC method, a line segment with a slope is used to approximate the interface in each cell with free surface (with γ greater than zero and less than one). Each line segment is defined by $C = \mathbf{n} \cdot x$ where C is the line constant, x is the position vector on the line and $\mathbf{n}$ is the unit vector normal to the interface. By doing the gradient of γ it can be determined the normal direction of the line segment as follows $\mathbf{n} = \frac{\nabla\gamma}{|\nabla\gamma|}$. To obtain that gradient, for instance of a triangular mesh as it is shown in Figure 11, firstly the algebraic average volume fraction at the three vertexes is calculated, and secondly the gradient from the average value of volume fraction. About how to approximate the volume fraction in the present interface cell from its nearest neighboring cells there are three ways to do it that are explained in detail in [62]. After the the normal direction is calculated, the position of the line segment from the mass flux between cells is computed by one of the method described in [62], and the mass flux across each cell boundary is obtained with Equation 12. These steps are repeated until the end time is reached.

In view of all that has been set out above IsoAdvector is not impeded to hexahedral meshes as quite a few of the current VOF algorithms. The main constraint is that the geometrical considerations named above only have sense when the Courant number is less than unity. However, it will be seen that the present simulations meet that requirement. About the operability of IsoAdvector it can be said that it is the same as any other solver, therefore the directories and the PISO algorithm described in the before Section (3.2.1) are equals. Nonetheless, an example of the code can be checked in the article by Johan Roenby et al. (2017) [63].

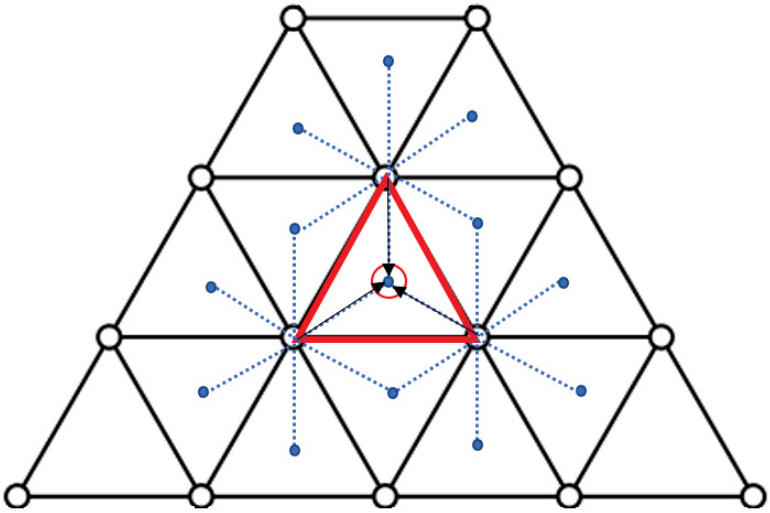

Figure 11: Calculation of the volume fraction gradient

3.2.3 CompressibleInterFoam

The CompressibleInterFoam solver can be applied in cases involving compressible, non-isothermal and immiscible two-phase flows. The solver algorithm used is MULES as in interFoam. CompressibleInterFoam has the capability of running cases where heat transfer and bubbly flows happen together, and they are very important in the current industries (as it has already been said in the first Section 1. Besides, OpenFOAM provides an interesting function called wallHeatFlux which calculates the heat flux at wall patches.

In the /0/ directory the variable temperature is added and in /constant/ the thermophysical properties of both species. Besides, it can be chosen how the species react (or if there is not reaction), the equation of state used for each fluid (perfect gas, perfect fluid, linear, etc), the composition of each constituent, and the thermodynamic (heat of fusion, heat capacity, etc) and transport (Prandtl number, viscosity, etc) attributes. Even, it may be defined polynomials for the equations of state, thermodynamic and transport properties.

Concerning the governing equations, apart from those explained in 3.1 another energy equations are added to these ones, but they are out of the scope of the thesis. More information about the solver can be found in the Master thesis written by Alessandro Manni (2014 [64].

3.3 Discretization methods

In this section, the different numerical schemes used in the simulations are explained. Naturally, all of the discretization methods available in OpenFOAM will not be described, inasmuch as the vast quantity of them. Besides, the majority of the descriptions are short and concise, on account of the methods are well-known or they could easily found on the web. It should be taken into account the huge impact that numerical methods have in the solution. They may provide different solutions, broadly, they have influence over the convergence, the accuracy and the simulation time. The naming utilized here is adapted to that used in OpenFOAM (as the file /fvSchemes/, see Figure 9).

- ddtSchemes (first time derivative terms $\frac{\partial}{\partial t}$): Regarding Section Governing equations 3.1 the two first terms of Equations 12 and 8 should be here: $\frac{\partial \rho \mathbf{U}}{\partial t}$ and $\frac{\partial \alpha}{\partial t}$.
  - Euler: transient, first order implicit, bounded.
  - Backward: transient, second order implicit, unbounded.
- gradSchemes (gradient terms ∇): the only gradient term is the pressure in Equation 8: $-\nabla p$.
  - Gauss linear: second order linear interpolation which requires the interpolation of values from cell centers to face centers.
- divSchemes (divergence terms $\nabla \bullet$): they are the majority as it shown:

  $\nabla \bullet (\rho \mathbf{U}\mathbf{U})$, identified as div(rhoPhi,U) in OpenFOAM.

  $\nabla \bullet \Big(\rho\nu \left[(\nabla \mathbf{U})^T - \frac{2}{3}\mathrm{tr}(\nabla \mathbf{U})^T \mathbf{I}\right]\Big)$, abbreviated as div(((rho*nuEff)*dev2(T(grad(U))))).

  $\nabla \bullet (\alpha \mathbf{U})$, formulated as div(phi,alpha).

  $\nabla \bullet (\alpha(1-\alpha)\mathbf{U}_r)$, written as div(phirb,alpha) in OpenFOAM.
  - Gauss linear: second order, bounded.
  - Gauss gamma V 0.1: it is a blend of central difference and up-wind. The 'V' means vector, so it is only used for vector fields, and the number goes from 0 (pure central difference) to 1 (pure up-wind).
- snGradSchemes: component of gradient normal to a cell face. The basis of the gradient calculation at a face is to subtract the value at the cell center on one side of the face from the value in the center on the other side and divide by the distance. The calculation is second-order accurate for the gradient normal to the face if the vector connecting the cell centers is orthogonal to the face.

  - Corrected: Second-order (Gauss linear) for maximum non-orthogonality above 70 degrees.

- laplacianSchemes (Laplacian terms δ): concerning the governing equations 3.1 there is only one term with a Laplacian operator: $\rho\nu\Delta\mathbf{U}$.

  - Gauss linear corrected: same as linear in snGradSchemes.

- interpolationSchemes: interpolations of values typically from cell centers to face centers.

  - Linear: Gauss linear (second order, unbounded).

With all this it has become clear how each term of Equations from 8 to 12), which define the samples, will be solved by OpenFOAM.

4 Simulations

4.1 Boundary conditions

The boundary conditions (BCs) used for next cases are common, due to all of them describe a single bubble in an column of water. The boundary consists of the atmosphere, on the top of the column of water, and the walls. The column of water is open to the atmosphere. Table 1 shows the used conditions. The meanings of the boundary conditions adopted in the cases and its values, when they are needed, are explained in the next paragraphs.

BOUNDARY CONDITIONS	Velocity (U)	Water fraction (alpha.water)	Pressure (p_rgh)
Wall	No slip	zeroGradient	fixedFluxPressure
Atmosphere	pressureInletOutletVelocity	inletOutlet	totalPressure

Table 1: Boundary conditions of the case

Regarding to the velocity:

- No slip condition fixes to zero all the values of the vector velocity.
- The pressureInletOutletVelocity applies zero gradient on all components, except where there is inflow, in which case you fixed the value of the tangential component. The value of the tangential component was fixed to zero.

Concerning the water fraction, which it is one for the water phase and zero for the air phase:

- As its name indicates, zeroGradient implements that the alpha water derivative with respect to the normal vector is zero.
- inletOutlet condition applies zeroGradient condition when the fluid flows out the domain (outwards), and you fix the value when the fluid flows in the domains (inwards). That value was set to zero.

With respect to the pressure, which is defined as the total pressure minus the hydrostatic pressure ($p_r gh = p - \rho gh$):

- The fixedFluxPressure boundary condition adjusts the gradient to zero accordingly with the velocity boundary condition, gravity forces and surface tension.
- In the totalPressure condition you fix the value of the pressure ($p0$) for the fluid that flows outwards. Automatically the pressure for the fluid that flows

in the domain is set to $p = p0 - \frac{1}{2}\rho|U|^2$. In the cases $p0$ was fixed to zero.

4.2 Grid resolution and selection of solver

It is known the huge importance of the domain size and grid resolution in computational fluid dynamics, because the credibility of the results is mainly based on both. Furthermore, these take a deep role in bubbly flows, since the size of the bubble can be small compared to the grid resolution. Therefore it is necessary to have a fine grid in the bubbly stream for running a proper simulation. At first glance it might seem a trivial task, it would only consist on design a mesh with a great number of cells. However, it is not an easy question, it is more complicated because as grid accuracy increases simulation time does the same. Therefore the objective here is to find a balance between grid accuracy and simulation time.

Another question is how to check the mesh resolution. There are lot of different ways, from compare the simulation results with experimental data to check your simulation with analytical data. The latter option used to be too complicated occasioned by the difficult of solving the proper equations to obtain the exact solution. In view of that, the analytical solution is commonly calculated through numerical methods, where an error is always made. OpenFOAM operates with numerical methods too, for this reason to check the simulation with analytical data has been neglected.

Finally, it was decided to simulate an easy case, called here "Bubble case", where a bubble rises in a liquid. Then it was compared to one article [5], which studies the dynamics of an initially spherical bubble rising in quiescent liquid. That article [5] was chosen due to all the 2D cases have also been simulated and checked in 3D. That allows to run 2D simulations instead of 3D keeping the correctness of the three dimensions. Furthermore, the numerical results of this articles has been validated against the theoretical results obtained in [31] , as well as with the experimental data shows in [65] .

Apart from the above, the choice of the solver plays a fundamental role in the simulation results. There are a huge number of algorithms available in OpenFOAM, see Section 3.5 of the OpenFOAM user guide [66]. For this thesis, the convenient solvers corresponds to the multiphase flow (see Subsection 3.5.4 of the OpenFOAM user guide [66]). The present thesis only covers case studies where the Mach number is significantly lower than 1, consequently the flow can be considered incompressible and isothermal because the change in the density is too small to take it into consideration [40]. Wherefore, based on the multiphase flow solvers it was chosen interFoam as the suitable one, in the first instance. The characteristics of interFoam are defined in Section 3.2.1. All the details of the case are presented in the next Section (4.2.1).

4.2.1 Bubble case

In this section the set up of the case is going to be described with an extensive detail, so that it could be reproduced similarly. The dimension of the case and the axes are defined in Figure 12, where D is equal to 1 centimeter, the red region refers to the liquid and the blue one to the gas.The properties of the gas phase corresponds to air and the properties of the liquid to water at 21°C.

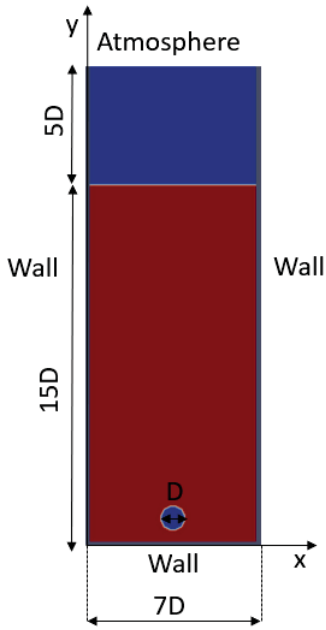

Figure 12: Dimensions of the bubble case. $D = 1cm$.

The selection of the domain sizes should not affect the results, except the bubble diameter. Consequently, more often than not the results do not depend on the dimensions, however it must be taken into account that the possible interactions between the bubbles and the walls would change the results. According to Sancak Özdemir (2005) the velocity of the bubble is mainly a function of the gravity, densities, surface tension and its diameter [67].

The values of the properties of both species can be seen in Table 2. The boundary conditions have been already fixed in Section 4.1.

PROPERTIES	Density (kg/m^3)	Kinematic viscosity (m^2/s)	Surface tension coefficient (N/m)
Air	1	1.48E-05	0.07
Water	1000	1.00E-06	

Table 2: Properties of species.

Relative to the numerical schemes, the methods used in the simulation are mentioned below (the features of each method are explained in the Section 3.3):

- ddtSchemes: Euler.
- gradSchemes: Gauss linear.
- divSchemes: Gauss Gamma V 0.1 for the velocity field and Gauss linear for the others variables.
- laplacianSchemes: Gauss linear corrected.
- interpolationSchemes: linear.
- snGradSchemes: corrected.

On the subject of the time simulation and input/output control:

- endTime 2.
- deltaT 0.001.
- writeControl adjustableRunTime.
- writeInterval 0.001.
- runTimeModifiable yes.
- adjustTimeStep yes.
- maxCo 1.

Hence the simulation reproduces 2 seconds (real time) remaining a maximum Courant number of 1 ($Co = \frac{U\Delta t}{\Delta x}$). Where U is the velocity in each cell, Δx refers to the grid size and Δt corresponds to deltaT, however, the command adjustTimeStep adjusts deltaT to ensure a Courant number less than the maximum. The Courant number has been defined only in one axis (-x axis) due to for this case, the value of Co does not depend on the direction. That is as a result of the mesh configuration. As is shown in Figure 13 the shape of the grid is a network made of squares, so each cell has identical length (Δy) and width (Δx). Last but not least, the gravity force was set to a value of 9.81 $\frac{m}{s^2}$ and the simulation type is laminar.

4.2.2 Results

The first step was to reach the grid size or grid accuracy needed to simulate cases which reproduce the reality. The method utilized is trivial: to increase the grid accuracy until the value of the water fraction is 1 or 0. It cannot be values of the water fraction between that numbers due to both fluids are immiscible, ergo intermediate values should be avoided.

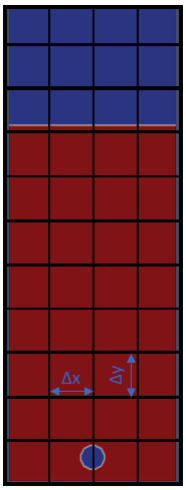

Figure 13: Pattern of the grid.

All the cases that have been run are as it has been described in the Section 4.2.1 (remember that D is equal to 1 centimeter, the red domain corresponds to liquid phase and the blue one to gas phase). The only difference between them is the grid accuracy and the solver used for running the simulation. Firstly, it was simulated a case, which it is called case 1, with a grid size $\Delta x = \Delta y = D/10$. The results are shown in Figure 14. As can be noted from the figure the accuracy of the two solvers is not enough, due to there are huge domains where the water and the air are mixed.

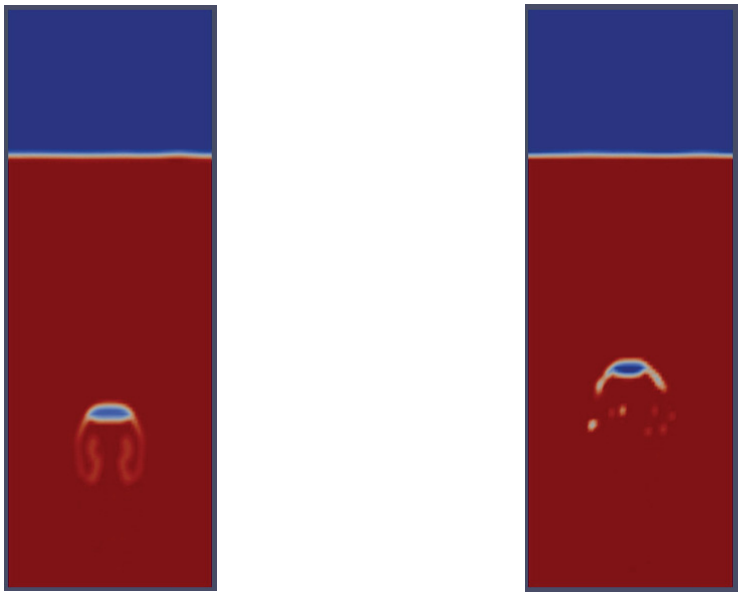

(a) interFoam (b) IsoAdvector

Figure 14: Case 1 at time 0.3 seconds.

Secondly, it was run the case 2, in which the grid size is the double of the one used in the case 1. That implicates $\Delta x = \Delta y = D/20$. The solutions can be seen in Figure

15. It can be appreciated the huge difference between interFoam and IsoAdvector, the latter one provides less white zones, which refers to the zones where the two phases are blended (miscible zone), than the first one.

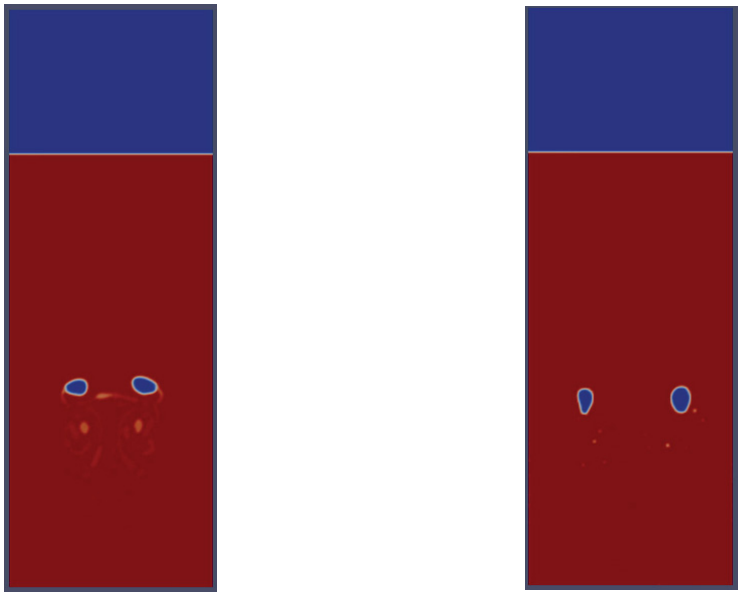

(a) interFoam (b) IsoAdvector

Figure 15: Case 2 at time 0.3 seconds.

On this point, it may think that the grid accuracy is good enough as long as IsoAdvector is the solver chosen, seeing as how the miscible zone could be ignored. Then this result (the case 2 simulated with IsoAdvector) was compared with the data shows in [5]. As mentioned above that article provides reliable data in 2D because each 2D simulation have been matched and checked with 3D simulations, which in turn has been checked with theoretical [65] and experimental [31] data. The density and viscosity ratios (ρ_r and μ_r respectively), both describe as the propertie of the gas phase divided by the same propertie of the liquid phase, set in the bubble case are equal to those define in the article [5]: $\rho_r = 10^{-3}$ and $\mu_r = 10^{-2}$. In consequence, the comparison between the case 2 simulation with IsoAdvector and the article [5] is correct.

Knowing that ρ_o is the density of the water (1000 $\frac{kg}{m^3}$), g is the gravity force (9.81 $\frac{m}{s^2}$), R means the ratio of the bubble (0.5 cm) and μ_o corresponds to the dynamic viscosity of the water ($1 \cdot 10^{-3} Pa \cdot s$), is directly to calculate the Galilei number and Eötvös number: Eo=3.5, Ga=1104. Once Galilei and Eötvös numbers had been calculated, it can be predicted the shape and behavior of the bubble. Accordingly with the explanation about the regions and the Galilei and Eötvös numbers calculated, the bubbles belong to the bubble case are in the region IV. Particularly, in the second sample defined in this region (low-medium Eötvös number and high Galilei number). Accordingly, the bubble should reach a constant shape and rise velocity with time, nevertheless the simulation of the bubble case 2 with IsoAdvector (Figure 15 did not

work proper. The bubble completely breaks up or divides, as can be seen in Figure 15, in two bubbles, not in a huge amount of satellite bubbles.

For all that the bubble behavior belongs to the region V, even if its shapes are not completely fit with the ones shown in the article (see Figures 16a and 16b), both bubble behaviors have similar developments. As a results of the quite different between the Eötvos and Galileli numbers of the two cases shown in the Figures 16a and 16b, Eo=1104 and Ga=3.5 against Eo=200 and Ga=70.7, both pictures do not match exactly, however it can be said that the two bubbles rise as region V bubbles do. Therefore, the grid size of D/20 is not enough for this kind of samples. Then, the third case was simulated with a fine grid $\Delta x = \Delta y = D/40$. The results are shown in Figure 17. As in the preceding cases it can be seen how IsoAdvector works better than interFoam under the same mesh since the first one represents less miscible zones (the white domains) and simulates better what here it is called above satellite bubbles.

(a) Case 2 with IsoAdvector.

(b) Region V. Source: [5]

Figure 16: Time evolution of bubbles.

As it can be seen in Figure 18 and **??** the results obtained with the fine mesh in IsoAdvector are close to the ones presented in the article [5]. In spite of the difference between Eötvos and Galilei numbers, Eo=1104 and Ga=3.5 against Eo=20 and Ga=70.7 for the case 3 and the article case respectively, both behavior are quite similar. This result sustain that a grid accuracy of D/40, where D is the diameter of the bubble, is enough for running those samples much the same a single rising bubble. Once the exactitude of both solvers, interFoam with IsoAdvector, was compared it shall be commented the execution time. The totally cases have been run in the same computer, consequently the comparison between the simulation time has sense. The computer used to run the simulation has a processor Intel®Xeon®E3 v5 Family with a base frequency of 3.4GHz and 4 cores. In Table 3 is shown the execution time, which means the time that the computer was running, of the whole cases. All of these have been simulated without using parallel computing, except the third case with IsoAdvector.

It can be appreciated in the said table how IsoAdvector takes more time than interFoam under the same factors. When the number of cells is not too much (up to 60.000), the execution time of the solver IsoAdvector is a bit more than the

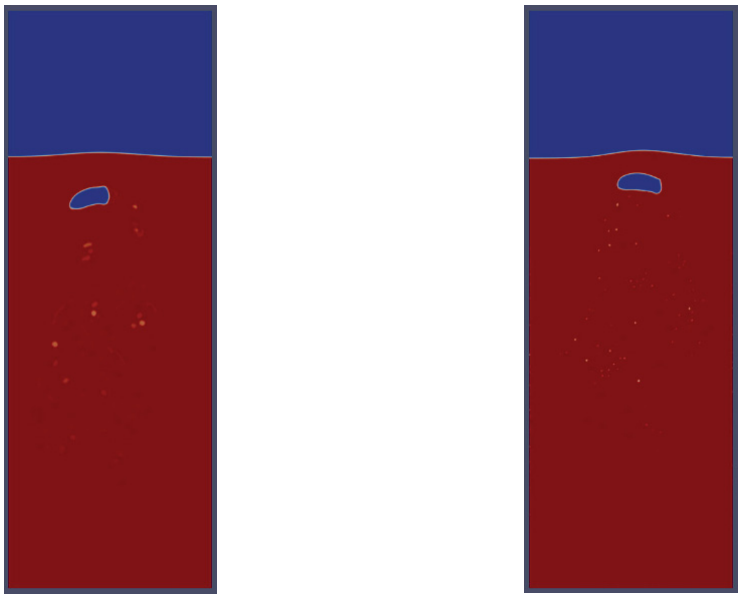

(a) interFoam (b) IsoAdvector

Figure 17: Case 3 at time 0.7 seconds.

(a) Case 3 with IsoAdvector. (b) Ga=70.7 and Eo=20. Source: [5]

Figure 18: Time evolution of bubbles in region IV.

double of the interFoam one. However that issue is quite easy to solve using parallel simulations, due to thanks to Aalto University I have at my disposal 16 available cores, which implicates that up to 1 million cells (60.000 cells per core) will not have vastly differences in the running time. Notwithstanding that the Mach number ($M = \frac{U}{U_s}$), where U is the object velocity (the bubble speed in this case) and U_s the speed of the sound, is about the order of $1 \cdot 10^{-2}$ (it was calculated with the online calculator available in [40]), the solver compressibleInterFoam was used to run the third case of the bubble case. The main features of this solver are described in the Section 3.2.3. The principal point to remember here is that the compressibility effects and the heat exchange are taken it into consideration by the solver.

The set up with this solver changes a little respect the one defined in 4.2.1, since new variables are introduced (as temperature and total presssure) and the value of the

CASE	Number of cells	Grid size (cm)	interFoam time	IsoAdvector time
1	14,000	0.1	5 min	11 min
2	56,000	0.05	9 min	20 min
3	224,000	0.025	10 hours and 30 min	7 hours*

Table 3: Executions time. *It was run in a parallel computing using 4 cores.

pressures affects the results. Therefore, new boundary conditions were introduced as the new files needed (see Section 3.2.3), but the grid size keeps its configuration. It have not been defined with the exactness of the Section 4.2.1 the settings used in this case, because there are lot of similarities with what has already been described. Although it is trivial to establish this case with an enough precision looking at Figure 19 and knowing that the equations of state used were perfect gas and perfect fluid for air and water each to each. As could be expected, the result of this simulation is quite analogous to the IsoAdvector one. Which can be checked seeing Figure 20, where both times corresponds to 0.7 seconds. Therefore, one may conclude that it is totally right to neglect the compressibility and the heat exchange in the analysis of a single rising bubble.

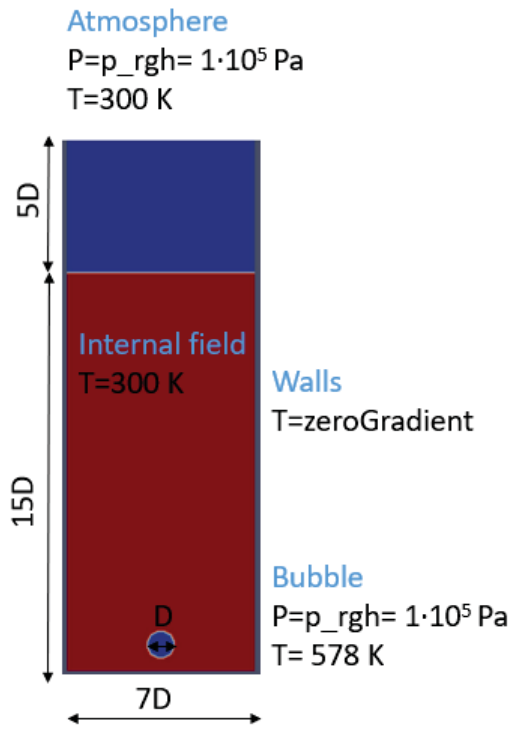

Figure 19: Setting of the bubble case with CompressibleInterFoam.

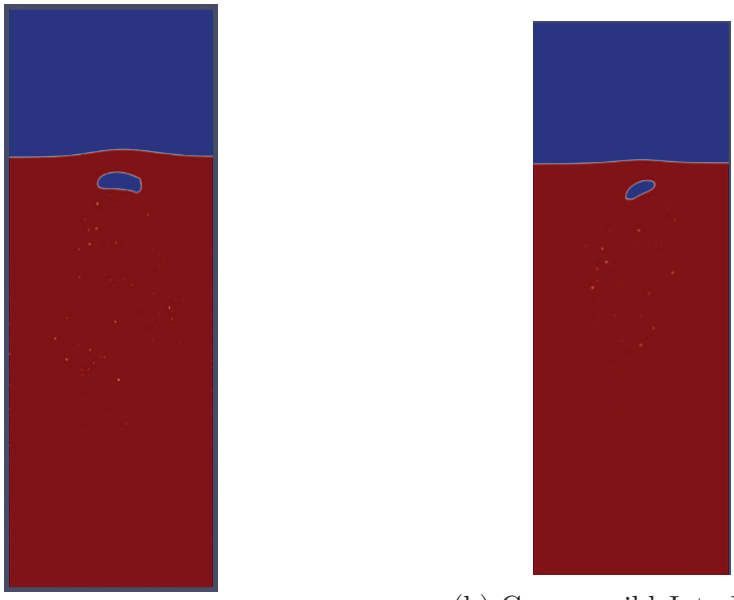

(a) IsoAdvector.

(b) CompressibleInterFoam.

Figure 20: Bubble case 3 at time 0.7 seconds.

4.2.3 Conclusions

Based on the above, the points below can be asserted:

- All the kinds of samples similar to the bubble case (see 4.2.1) are able to be run with the solver IsoAdvector.
- The grid accuracy should be at least the diameter of the bubble divided by forty, then simulations could be used as an investigative tool for studying a single bubble rise and the balance between accuracy and time execution is adequate.
- The results of these samples are not depend on the thermal and compressibility effects.

4.3 Investigated case: single bubble rising

This investigated case was chosen as a result of the proximity with the bubble case. This similarity allows to simulate the case under comparable circumstances. In addition, as it has already been proven in 4.2, proper grid size and solver are known to reach decent outcomes. For ensuring the validity of the results obtained, these will be compared with the experimental data shown in this article [8]. That article was chosen due to the experimental data was extracted from a test which, for a priori, can be simulate with a two dimensions mesh. The experimental test consists of a rectangular column (which is 0.3 meters wide, 3 meters height and 5 meters deep) with a system air-water that provides a single bubble rises in water.

Seeing the dimensions of the rectangular column it can be maintained that a 2D simulation will match with the experimental results. Even though in Section Concluding Remarks of this article [8] it is emphasized that their 2D simulations are analogous to the test measures, it is always interesting to acquire similar results with another software. Furthermore, there is experimental data in the article obtained through experiments in cylindrical columns (see FIG.4 in [8]) which does not match with their simulations done. Therefore, it is presented a good opportunity to run 3D simulations that coincide with these data, which will be called 3D experimental data.

In conjunction with the last paragraphs, it will be contrasted an open-source software with a commercial one, due to the software used in the article [8] is ANSYS-CFX. As it is shown in the article [13], above mentioned in 1, predictably OpenFOAM and ANSYS-CFX will yield equally.

4.3.1 Set up 2D

In this section the set up of this case is going to be described with an extensive detail, as it was done in the Section 4.2.1. The dimension of the case and the axes are defined in Figure 21, where D is the diameter of the bubble and D_T is equal to the column diameter, both will be defined for each subcase. As it has been before, the red domain refers to the liquid phase (water) and the blue one to the gas phase (air).

The size of the case have been fixed in accordance with the one used in the article [8]. The properties of the substances are shown in Table 4, which also are in accordance with [8]. The boundary conditions used in this case have been defined in Section 4.1. Moreover the initial values of all the magnitudes (velocity, pressure and water fraction) have been set in the same section. Regardless of the atmosphere pressure has a fixed value of 101.325 kPa in the article [8], that value was set to zero in these simulations since it was demonstrated (see 4.2.2) that the compressibility effects do not influence the outcomes of the simulations.

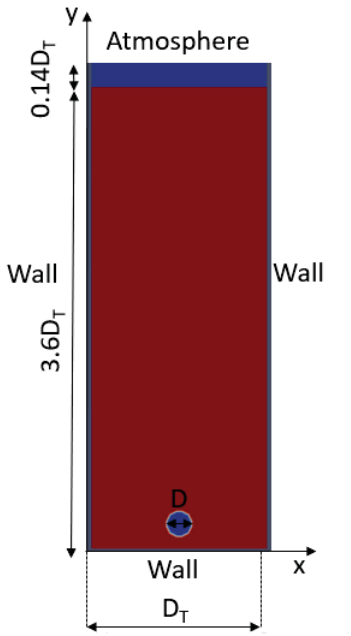

Figure 21: Set up 2D single bubble rising.

PROPERTIES	Density (kg/m^3)	Kinematic viscosity (m^2/s)	Surface tension coefficient (N/m)
Air	1.29	1.32E-05	0.072
Water	998	1.00E-06	

Table 4: Properties of the substances.

Corresponding to the numerical methods, the schemes used in the simulation are mentioned below (the description of each method are shown in Section 3.3):

- ddtSchemes: backward.
- gradSchemes: Gauss linear.
- divSchemes: Gauss Gamma V 0.1 for the velocity field and Gauss linear for the others variables.
- laplacianSchemes: Gauss linear corrected.
- interpolationSchemes: linear.
- snGradSchemes: corrected.

As can be appreciated above, there is only one change in the discretization methods with respect to those used in the bubble case. This variation provides a better

running, adding a second order derivative with respect to the time. About the time simulation and input/output control are also close to the bubble case:

- endTime 0.8.
- deltaT depends on the case (see Table 5) .
- writeControl adjustableRunTime.
- writeInterval 0.005 (except when the bubble diameter is 4mm, then it is 0.004).
- writeFormat binary.
- writeCompression compressed.
- runTimeModifiable yes.
- adjustTimeStep yes.
- maxCo 0.5.

The Courant number is constant in the domain just as it happened in the bubble case. In fact, the grid configuration is exactly the same as it is shown in Figure 13. However, Co number was reduced to 0.5 for increasing the accuracy of the results, despite of the increase of the execution time. About the end time, 0.8 seconds should be enough based on the dimensions of the case (Figure 21 and Table 5) and the rise velocities (see TABLE1 in [8]). Concerning the grid sizes, the values are in Table 5, the coarsest grid is configured by cells with D/40 wide and height. Therefore, the mesh should provide decent results in concordance with the conclusions of the previous Section (4.2.3). Referring to those writeFormat and writeCompression values, they were chosen for reducing the data volume, then enhancing the data storage.

As it is shown in Table 5 the time steps used in the simulations were between 0.0005 and 0.0001 seconds, alike those used in the article [8] simulations. Besides, the characteristic time (t_c) is also in that Table (5), which is defined as the bubble diameter between the rise velocity. This time has a huge influence in the write interval, as a matter of fact, t_c fixes the write interval that provides a proper balance between a good visualization and the occupied storage space: being the write interval smaller or equal to the characteristic time divided by ten.

Due to t_c was fixed before running the simulation, the rise velocities obtained in [8] were used to calculate it. Once the characteristic time was calculated, all the write intervals were set to 0.005, as a result of mostly all these write intervals were slightly bigger than 0.005, except when the bubble diameter is 4 millimeters (then t_c takes a value of 0.004). Last but not least, the value of the gravity force and the simulation type remain constant: 9.81 $\frac{m}{s^2}$ and laminar respectively.

BUBBLE DIAMETER [D] (mm)	Column diameter [D_T] (mm)	Grid size [Δx] (mm)	Time step [Δt] (s)	Number of cells	Characteristic time [t_c] (s)
4	25	0.1	0.0003	233,750	0.04
5	25	0.125	0.0001	149,600	0.05
7	25	0.125	0.0002	149,600	0.06
8	25	0.2	0.0005	58,500	0.07
9	40	0.16	0.0003	233,750	0.07
12	40	0.16	0.0003	233,750	0.09
20	400	0.5	0.0004	2,393,600	0.07

Table 5: Settings of the subcases.

4.3.2 Results 2D

The cumulative continuity error is one of the most important things for checking if a simulation has been run in accordance with than you expected. The cumulative error is a summation of all the global continuity errors (from the first step). The global continuity error in turn is the summation of the errors in all the continuous variables (CVs) at present time, as a result of this the cumulative error should be enough small in comparison with the values of the CVs. The variables defined in this case are: pressure, water fraction and velocity. However the water fraction is not a continuous variable, because of its value is one or zero depending on the domain. For the single bubble rising case, fluctuations on the pressure are less important than in the velocity field, in view of the order of magnitude. In addition, a variation of one unit in the pressure, only one pascal, affects quite much less than the same variation in the speed, one meter per second. In view of that and the results of the rise velocity in the article [8] (it ranges from 0.1054 to 0.277 meters per second) the cumulative error should be at least on the order of $1 \cdot 10^{-3}$.

In Table 6 are shown the cumulative continuity errors, execution times and the number of cores used for each subcase. As it can be noted all the simulation errors are lower than $1 \cdot 10^{-3}$, consequently the solution is not affected by an accumulation of errors. In addition it can be seen that the highest execution time was ten hours. This is a quite small value if it is compared with the required CPU time of the article [8] (about two weeks for the subcase 7 mm with the same number of cells and time step). Surely, the reason is simply due to the high different between the computers used, in technological terms, and had no bearing on the software utilized. As might be expected, the execution time is longer while the amount of cells increases and the time step decreases. As a result of that, and bearing on mind the number of cores, the longest simulation corresponds to the one which has the lowest time step. However there are more parameters that affect the required CPU time, for instance, the grid resolution. As it can be seen in Table 6, the simulation times of

the 9 and 12 mm subcases are not equal, although the grid sizes, the time steps and the number of cores are alike. The reason of that is because the grid resolution of the latter subcase (12mm) is bigger than the other one (9mm), in terms of the bubble accuracy: D/75 against D/56 respectively.

BUBBLE DIAMETER [D] (mm)	Number of cores	Execution time	Cumulative continuity error
4	2	4 hours and 40 minutes	-1.77E-04
5	1	10 hours and 1 minute	-1.55E-05
7	2	7 hours and 21 minutes	-5.05E-05
8	1	1 hour and 45 minutes	-2.54E-04
9	4	4 hours and 45 minutes	2.24E-06
12	4	5 hours and 15 minutes	5.17E-05
20	10	2 hours and 45 minutes	1.22E-05

Table 6: Execution time and cumulative error.

Once having seen the time spent in the simulations and the cumulative continuity error, the next step is to compare the result with the article simulations. Firstly, the trajectories were compared at a glance, that was the rough method for checking the proximity of both simulation results. Secondly, the data was extracted, in particular the velocity field. Then the rise velocities were compared with the experimental data, for ensuring the validity of the results. Next Figures from 22 to 26 shown the simulation results of the rise trajectories of the bubbles in a column of water, OpenFOAM corresponds to the pictures in color and ANSYS-CFX with those in black and white. There are some subcases which have not been represent in a figure in consequence of they are not plot in the article either.

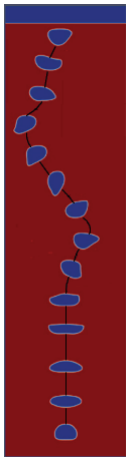

(a) Source: Present study.

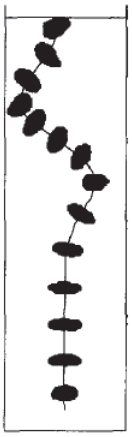

(b) Source: [8].

Figure 22: Rise trajectories of 4mm bubble.

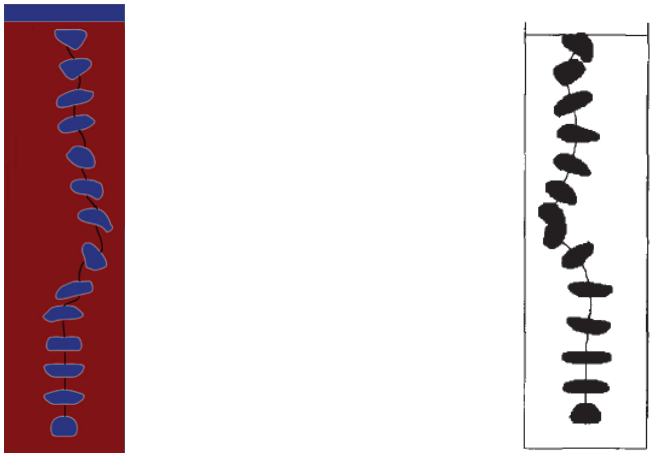

(a) Source: Present study. (b) Source: [8].

Figure 23: Rise trajectories of 5mm bubble.

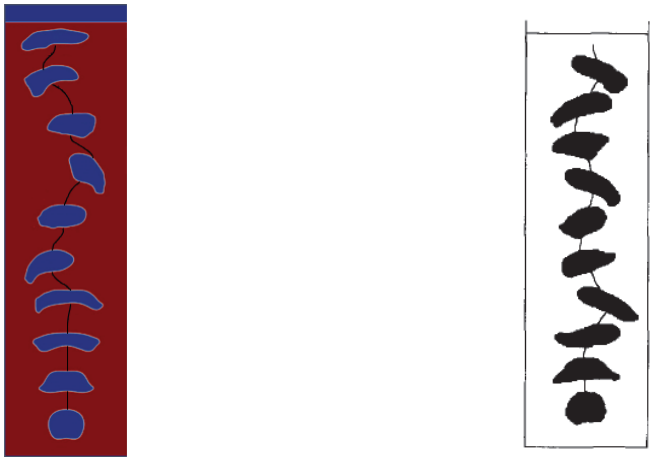

(a) Source: Present study. (b) Source: [8].

Figure 24: Rise trajectories of 7mm bubble.

On the one hand, in those figures there are some rise trajectories that are almost exactly the same, as the 4 (22), 12 (25) and 20 (26) mm bubbles. On the other hand, there is one of them, that corresponds to the 5 mm bubble (23), in which the rise trajectories are symmetric. In the last one (24, the rise trajectories of a 7 mm bubble are the most different ones in comparison with the others. As a result of those comparative relations, at first sight, it is hardly be able to come a conclusion. Therefore, seeing that the FIG. 3 in [8] represents the swing in the -x axis with the time, it is decided to plot something similar to that. Due to the precision of the data collected in that article is not so much (collecting data of a graph by hand), the data mining of our simulations was doing according to that. Hence, only the points where the trajectory of the bubble changes direction have been drawn, or in other words only the local maximums and minimums have been plotted. The result of that may be seen in Figure 27, where each color indicates each bubble diameter,

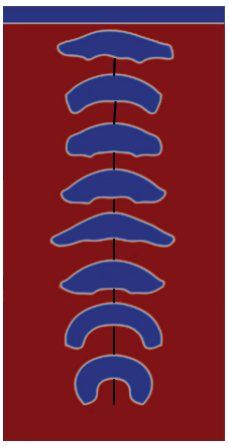

(a) Source: Present study.

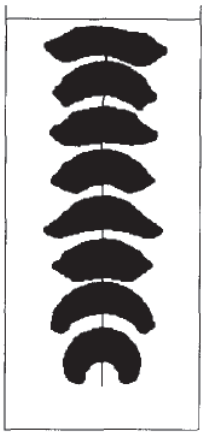

(b) Source: [8].

Figure 25: Rise trajectories of 12mm bubble.

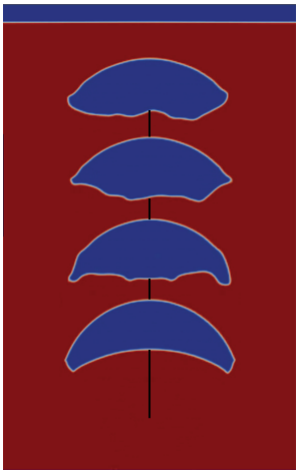

(a) Source: Present study.

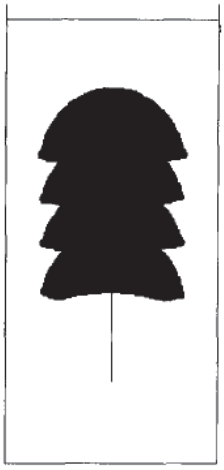

(b) Source: [8].

Figure 26: Rise trajectories of 20mm bubble.

the squares are our own simulations and the triangles the article ones. The bubbles whose diameters are twenty and twelve millimeters have not been plot due to its trajectories are straight lines.

On a slightly different note, I shall speak about the rise velocity. It has not found any official postprocessing function to obtain the rise velocity in OpenFOAM. They were located some files on the web, which calculate the velocity of the bubble in each time step. Notwithstanding, I misunderstood these directories, so it was decided to implement one method for getting the velocities values. It can be checked in Figure 27 how the highest and lowest absolute values of the trajectories (global maximums and minimums in absolute value) in the -x axis have similar values for both softwares. Additionally, the bubbles with equals diameters intersect the -y axis

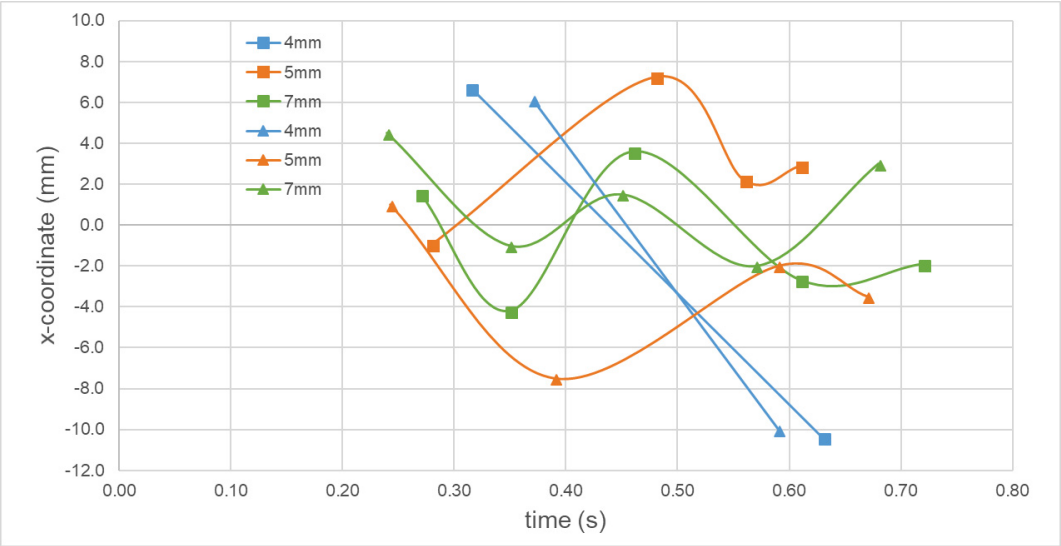

Figure 27: Local maximums and minimums of the bubble trajectories. Sources: Present study (squares) and [8] (triangles).

(see 27 when x-coordinate is zero) the same number of times. Nevertheless, the points where those absolutes values are reached do not match each other, consequently the intersection points with the -y axis either. In any case, with these results, it would be possible to estimate the maximum and minimum deviation of the trajectory with respect the -y axis and how many times the bubbles will go through the point $x = 0$. Notwithstanding, it is not possible to suppose a proper trajectory of the bubble due to the time for each point is unknown, what in these cases and similar ones is the same as the y-coordinate.

The procedure for each subcase consists on:

- 1. Extract the data of all the fields, for each time step.
- 2. Select all the fields whose volume fraction of water is equal to zero, for each time step.
- 3. Choose only the velocities which go in the -y positive direction and are major than the cumulative error (see Table 6), for each time step.
- 4. Calculate the average (arithmetic mean), for each time step (these averages are the rise velocities).
- 5. Take only the arithmetic average of those rise velocities that are within the domain $[0.85v_e, 1.15v_e]$, where v_r is the experimental velocity rise, calculated from Equations 13, 14 and 15.

The first point was done with ParaView and the others with a Matlab script. The last step had to be done due to the bubbles have abnormal behaviors, with regard to

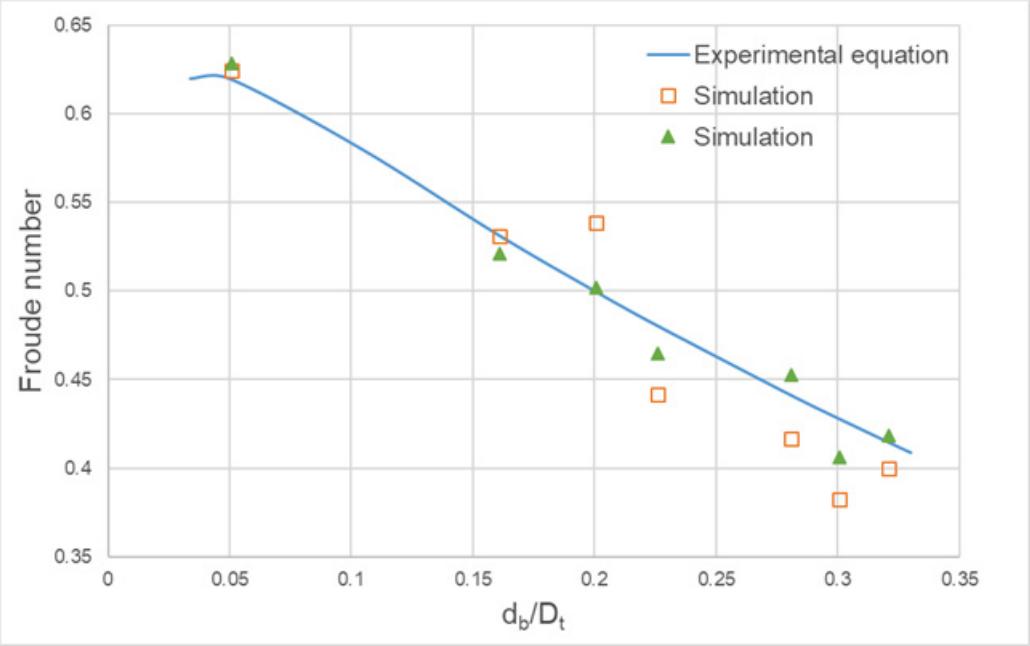

Figure 28: Rises velocities in 2D column. Sources: Present study (OpenFOAM) and [8] (ANSYS-CFX).

the rise velocity, in three cases: in the beginning, when they are near the wall and at the end (near the atmosphere). In these cases, the rise velocities should not be taken into account since the arithmetic mean would be affected so much, then the results would be disrupted. As can be seen in Figure 28 the procedure used to calculate the velocities works quite good. It should be taken into account that this method matches well with the experimental data because for all simulations reported here the bubbles neither gained nor lost more than about 10 percentage area during its rise [8]. Therefore, the little separated bubble fractions are not affected too much the arithmetic mean. Experimental Equations from 13 to 15 were obtained from the 2D experiments and simulations realized in [8] and they are closed to the those proposed by Collins (1965) [15]:

$$V_b = 0.62\sqrt{gd_b} \qquad \text{for } d_b/D_T < 0.07 \tag{13}$$

$$V_b = 0.62\sqrt{gd_b}(1.1exp(-1.55d_b/D_T)) \qquad \text{for } 0.07 < d_b/D_t < 0.4 \tag{14}$$

$$V_b = 0.236\sqrt{gD_T} \qquad \text{for } d_b/D_t > 0.4 \tag{15}$$

Where d_b is the bubble diameter and D_T the column diameter. With reference to Figure 28, the Froude number is equal to $V_b/\sqrt{gd_b}$. At a first glance it is difficult to situate the bubble diameters and the error committed looking at Figure 28. In consequence, Table 7 was made to see numerically the rise velocities and its errors with respect to the experimental equations. Table 7 shows small errors. All of them

(OpenFOAM errors) are less than the 10 %, which corresponds to the maximum gained or lost area by a bubble. As can be checked in the same Table the rise velocities between 4 and 8 mm do not follow a pattern, it seems that for these bubble sizes the rise velocity is independent of the bubble diameter. That theme is in conformity with some experimental evidence, as the ones exposed in these books [4] and [68], where it is demonstrated that the rise velocity of bubbles in the range from 3 to 10 mm are practically not dependent of the bubble size. In addition, looking at -x coordinate of Figure 28 it may be confirmed that the rise velocity of a single bubble in a column of water depends on the ratio of the bubble diameter to the column diameter. Finally, seeing both Figure 28 and Table 7 it could be said that the accuracy of OpenFOAM with IsoAdvector is better than ANSYS-CFX. Despite the absolute errors in OpenFOAM generally are smaller than in ANSYS-CFX, it should be taken into consideration that the last version of OpenFOAM has been used against the version ANSYS-CFX 4.1c, which is at least from ten years ago. In consequence of the last sentence, it should be only asserted that both softwares provide proper and similar results in the subject matter analyzed here. This similarity is also proven in [13].

BUBBLE DIAMETER [D] (mm)	rise velocity (OpenFOAM) (m/s)	rise velocity (ANSYS-CFX) (m/s)	absolute error (OpenFOAM)	absolute error (ANSYS-CFX)
4	0.1035	0.1054	1.8%	0.0%
5	0.1114	0.1195	0.6%	7.9%
7	0.1189	0.1095	2.7%	5.4%
8	0.1175	0.1123	1.0%	3.5%
9	0.1385	0.1315	3.1%	8.0%
12	0.1397	0.1316	5.0%	10.5%
20	0.279	0.2770	1.6%	0.9%

Table 7: Rises velocities in 2D column and absolute errors.

4.3.3 Set up 3D

As it has already said above, there is 3D experimental data in the article [8] that it has only contrasted with 2D simulations. Therefore, it is presented a good opportunity to set up 3D cases and to compare them with the experiments. The 3D data available in that article cannot be extracted with a high accuracy, it is not able to see exact values, as a result of the vastly amount of data plot in one graph (FIG. 4 of [8]) for the same bubble diameters. For that reason, apart from comparing the simulations with the experiments [10] and [8], they will be compared with some equations, which were constrasted with a great amount of experiments [6].

In Figures 29, 30 and 31 are shown (respectively): the shape of the case, its dimensions projected in a cross-sectional cut, whose normal vector is (0 1 0) and contains the point (0, 0, 0) and this plane (the green one). The column diameter (D_T) and the atmosphere height (w) will be set for each subcase. The properties of both species and the numerical methods used to run these simulations are completely identical to those defined in the 2D case: see in Section 4.3.1 Table 4 and the numerical methods exposed. Regarding the directory /controlDict/, almost all the times and input/output data settings are similarly to the 2D single bubble rising (see 4.3.1). Certainly all the settings are exactly the same except the end time, deltaT and writeInterval.

The time step (deltaT) was set to 0.0003 for every subcase. The end time was fixed in each subcase taking into consideration the rise velocities provided by the experimental data (between 0.2 and 0.25 m/s) and the dimensions of the case (see Figure 30 and Table 8). Regarding the writeInterval it meanly depends on the characteristic time. Such as it was done in Section 4.3.1, here the writeInterval of each subcase takes a value of t_c divided by 10. About the grid size theme, the 3D meshes are more complicated than 2D ones. Moreover, the cylindrical meshes are not made by hexahedrons. Due to the huge number of cells that a 3D may be presented, it is quite important to focus in the key regions of the domain. For that, it is important to know the future simulation behaviors or to do a good prediction about where the simulation will go. Then, the number of cells can be reduced, creating a fine mesh only in the key regions and a coarse mesh in the remaining domain.

BUBBLE DIAMETER [D] (mm)	Column diameter [D_T] (m)	Atmosphere height [w] (m)	Number of cells	End time (s)	Characteristic time [t_C] (s)
4	0.017	0.001	1496000	0.2	0.016
6	0.0255	0.001	987000	0.2	0.024
8.5	0.036125	0.002	1229200	0.4	0.034
12	0.051	0.002	229500	0.6	0.048

Table 8: Settings of the subcases.

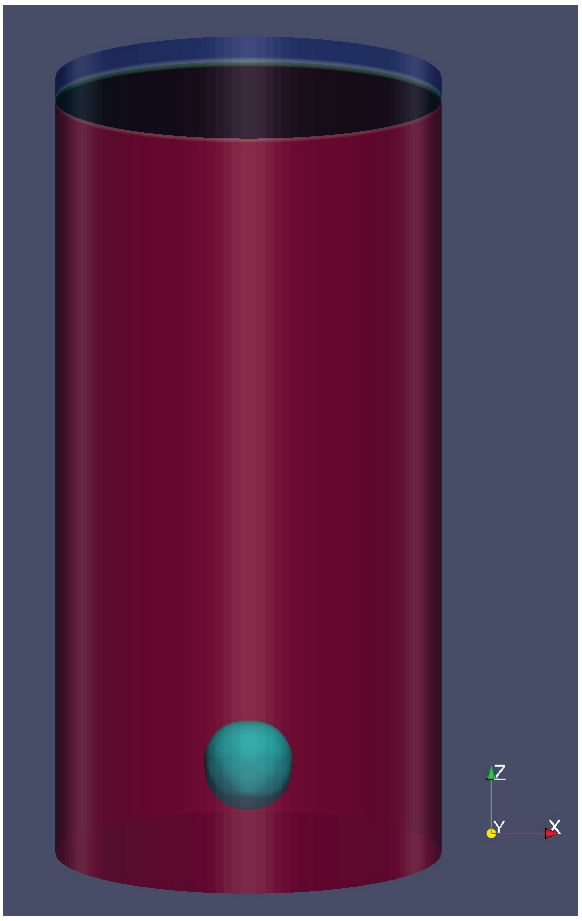

Figure 29: Shape of the case.

For these cases it was known beforehand where the fine and the coarse meshes should be located, since it can be predicted with enough accuracy the trajectory of the bubble as it is shown in Section 2.3. Based on the article [5] it could predicted that the trajectories are going to be close to an straight line, so the refinement is easier. Having in mind that different meshes were build for each subcase. An example of fine and coarse domains are shown in Figures 32 and 33. All the fine domains has an accuracy of D/40, they correspond to the polyhedron that encloses the bubble, while in the coarse domains have not been set any criteria. There are two subcases that have the fine grid until the top of the cylinder, these are 4 and 8,5 mm. However, the remaining two subcases (6 and 12 mm) has not the refinement the whole cylinder height, because of the results are similar, that is the reason why there are big differences in the number of cells of the subcases. Therefore the main point here is to refine enough proper the mesh in the beginning. OpenFOAM provides easy tools to refine the mesh in the region wanted. The produce consist in two files: the first one select the region indicated and the second applies the refinement in that zone.

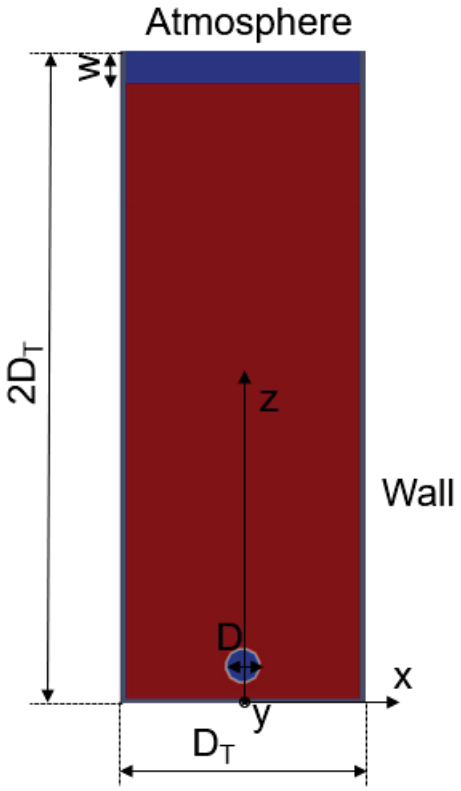

Figure 30: Set up 3D single bubble rising.

4.3.4 Results 3D

As it has been said in the commencement of Section 4.3.2, the cumulative error is the first data that it should be looked when the simulation is ended. Besides, the range of this error should be remained, at least on the order of $1 \cdot 10^{-3}$, inasmuch as the velocity values are in the same order than those in 2D. Table 9 shows the cumulative continuity errors, execution times and number of cores used for each subcase. As it can be perceived the highest cumulative error ($-1.84 \cdot 10^{-3}$) is in the adequate order, in consequence the solution is not affected by an accumulation of errors. With regard to the execution times despite of the vastly amount of cells compare to the two dimensions case (6), about the quadruple or quintuple, these times are quite parallel. The reason of that is due to the size of the fine mesh is similar in both cases, since the 2D case has a fine grid in the whole domain and the 3D case only in the refined regions. About the rise velocities, as it said above, apart from comparing the simulations with the experiments [10] and [8], they will be compared with some equations, which were constrasted with a great amount of experiments [6].

In the simulations done, like it was predicted, the bubbles raise upwards in a vertical line. This allowed to extract the data in an easy manner: dividing the path between the time. Besides, the time accuracy provided by OpenFOAM is the proper one. Figure 34 shows the results of the simulations, experimental data and numerical

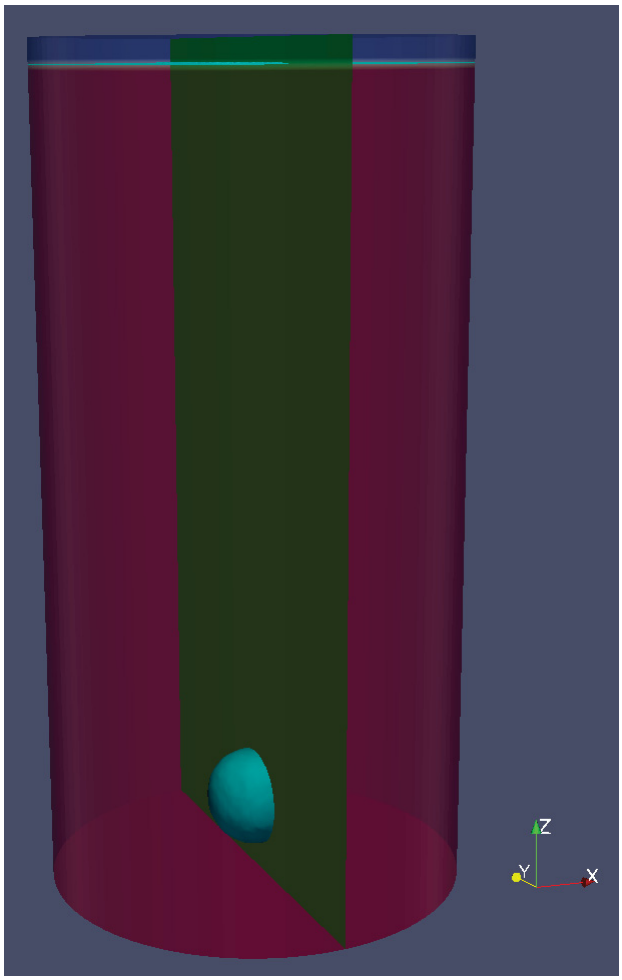

Figure 31: Cross-sectional cut. The bubble is cut right in its middle.

BUBBLE DIAMETER [D] (mm)	Number of cores	Execution time	Cumulative continuity error
4	16	12 hours and 6 minutes	-2.17E-04
6	16	5 hours and 29 minutes	-1.69E-03
8.5	16	9 hours and 17 minutes	-4.28E-04
12	4	2 hours and 5 minutes	-1.84E-03

Table 9: Execution time and cumulative error.

ones. It can be noted how the simulation results are closer to the equation than the experiments. The reason of that is because the experiments should have done with tap or contaminated water instead of filtered or distilled one. In the article [10] it is clear that the experiments were carried out with water, however, in the other one [6] it is not said. Nonetheless, what it have been said it is considerably probable, since the rise velocity of the bubbles are smaller in tap or contaminated water, as it is

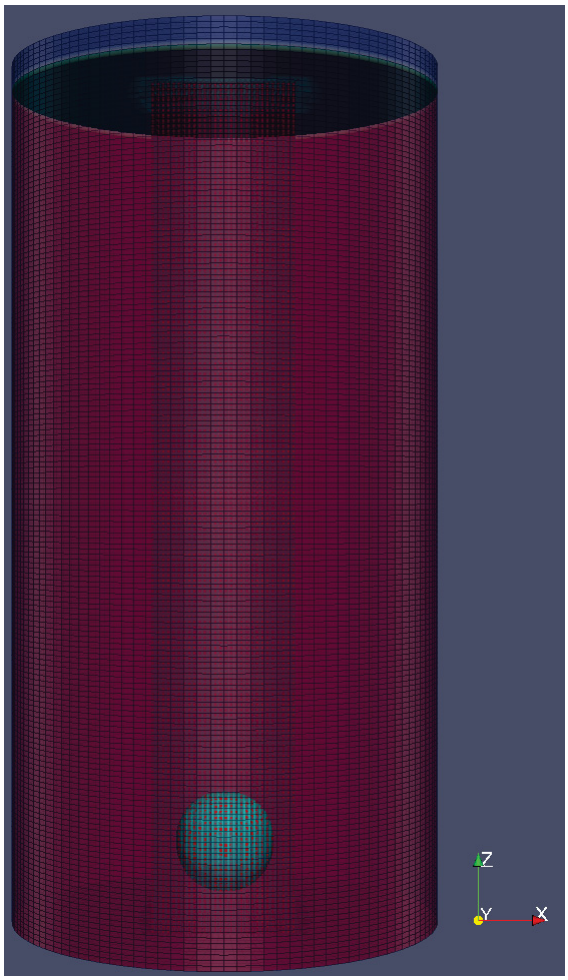

Figure 32: Front view of the mesh grid.

proved in [16].

To enhance the understanding of Figure 34, Table 10 has been made. The errors of the simulations with respect to Equation 4 are enough low to validate the set up established. Additionally, the maximum velocity rise error happens in the same bubble diameter (12 mm) and it has the same order (about 5 %), as the 2D case (compare Tables 10 and 7).

Finally, it will be check out the shapes of the bubbles and the trajectories with the predictions done in the article [5].Firstly, taking into account that the highest end time is 0.6 seconds and accordingly to the results shown in that article, the trajectories should be straight lines, and they are. Secondly, calculating the Eo and Ga non dimensional numbers the bubbles are near to the boundary of two regions, expect the 4 mm bubble diameter which belong to the region II; or they are out of the graph, which happens to the Ga numbers of 8.5 mm and 12 mm bubble diameters. There is an issue here, since the density and viscosity ratios of the simulations are similar to the articles ones, but they are not equal. As a result of that the boundaries

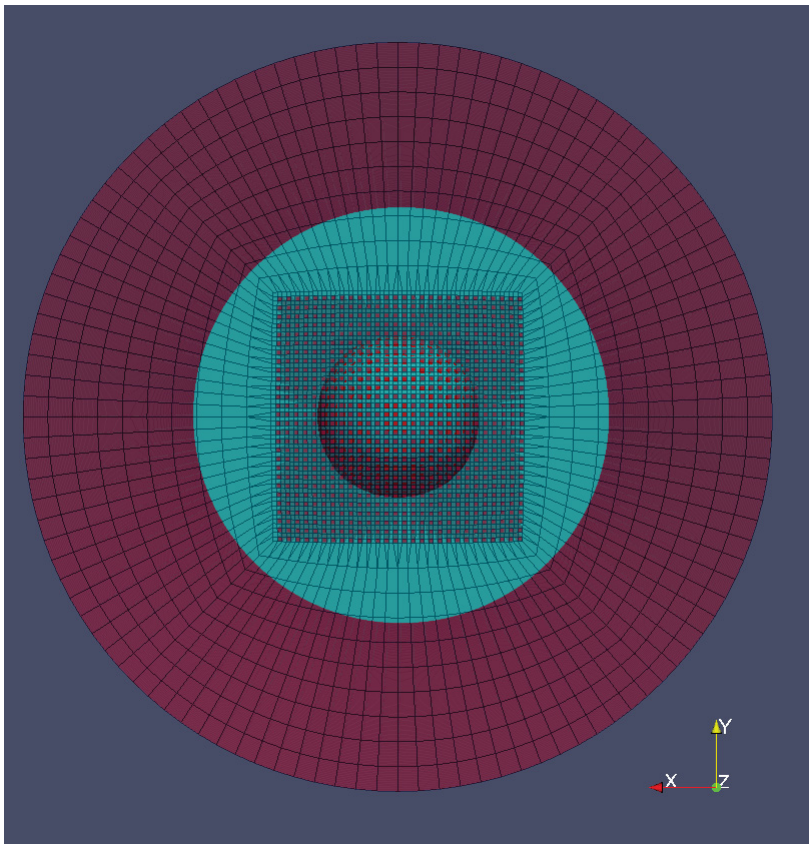

Figure 33: Top view of the mesh grid.

BUBBLE DIAMETER [D] (mm)	Simulations (m/s)	Experiments (m/s)	Experimental (m/s)	Equation (m/s)	Error
4	0.2698	0,2167-0,2417	0.2438	0.2710	0.43%
6	0.2487	0,2-0,2375	0.2250	0.2558	2.77%
8.5	0.2514	0,2-0,2333	0.2375	0.2590	2.94%
12	0.2615	0.2333	-	0.2772	5.65%

Table 10: Rise velocities error in 3D column. The errors were calculated with the simulation values respect to the equation values. Source: Present study (Simulation), Equation [9], Experiments [8] and Experimental [10].

may be changed.

In spite of that problem, the shapes of the bubbles have been compared with those shown in [8] to find out the corresponding region. Figures 35, 36 and 37 confirm that the bubbles of 4 , 6 and 12 millimeters of diameter belong to the regions II, IV and V, respectively. Besides, it can be affirmed that the bubble of 12 mm is close to the boundary of region IV, accordingly to the ejection of small satellites before the change of topology (to a doughnut-like or toroidal) [5]. In Figure 38 it can be seen that the bubble has characteristic of the regions IV and V, as a result of that, this

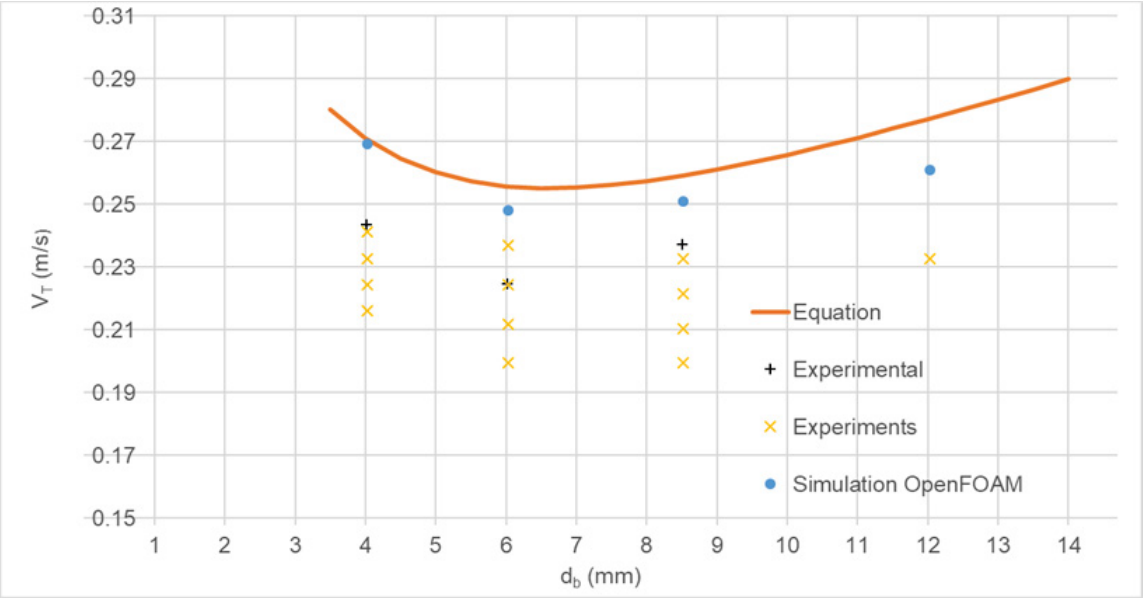

Figure 34: Rise velocities in 3D column. Source: Present study (OpenFOAM), Equation [9], Experiments [8] and Experimental [10]

bubble should be right in the boundary of these regions.

(a) Bubble region II. Source [5]

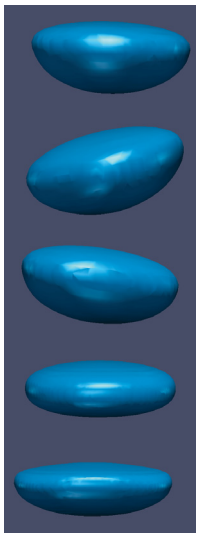

(b) Bubble diameter 4mm. Source: Present study

Figure 35: Time evolution of bubbles.

(a) Bubble region IV. Source [5]

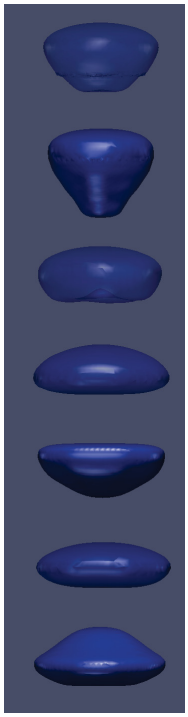

(b) Bubble diameter 6mm. Source: Present study

Figure 36: Time evolution of bubbles.

(a) Bubble region V. Source [5]

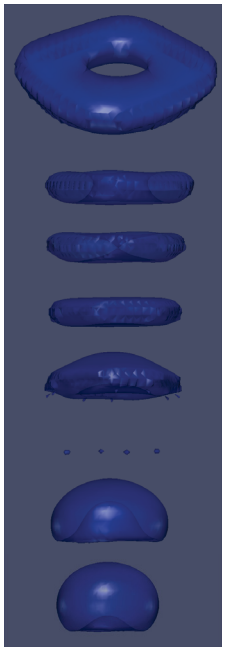

(b) Bubble diameter 12mm. Source: Present study

Figure 37: Time evolution of bubbles.

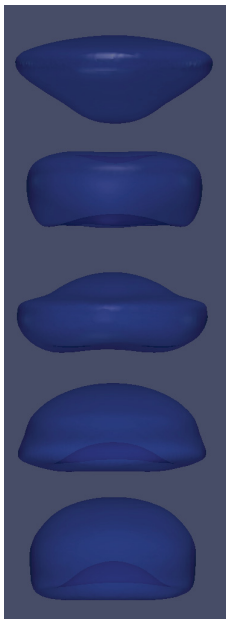

Figure 38: Bubble diameter 8.5 mm.

4.3.5 Conclusions

From the results presented in Sections 4.3.2 and 4.3.4 the following conclusions can be derived:

- OpenFOAM shown to be comparable to commercial codes, as ANSYS. See Figure 28 and Table 7.
- The maximum magnitude of the lateral migration and the frequency of a bubble can be predicted in the studied range, but the direction of the bubble is random. See Figure 27.
- The rise velocities were well calculated with the code implemented in Matlab. See Tables 7 and 10.
- The rise velocity errors of the 2D and 3D simulations are quite similar. See Tables 7 and 10.
- The bubble shape in the 2D simulations are not match with real ones, however it may be established a relation between 2D and 3D shapes.
- 3D simulations are in close agreement with the bubble shapes shown in [5], see Figures from 35 to 38.
- Some 3D shapes match with the real images, however, it is needed more literature to validate the entire range simulated. See Figures fromt 39 to 42.
- The rise velocity equations in 2D and 3D match quite well with experiments and simulations. See Figures 28 and 34.
- IsoAdvector is able to run proper simulations without an hexahedral mesh. See Figure 33.
- The simulations done represent distilled water. The rise velocities of the bubbles in tap water are lower than those in distilled water between an 8% and 12%. See Table 10 and Figure 34.

5 Summary and future works

OpenFOAM, an open-source M-CFD software, was chosen in order to simulate an initially spherical bubble starting from rest in a column of water open to the atmosphere in two dimensions. Two solver algorithms have been compared, InterFoam and InterFlow. Both solvers are for solving cases with two incompressible, isothermal immiscible fluids using a VOF phase-fraction based interface capturing approach. The results shown that the geometric VOF scheme isoAdvector, which is associated to InterFlow, works better than MULES, associated to InterFoam. Moreover, for these samples the results are independent on the thermal and compressibility effects. Besides, simulations results shown that the grid accuracy should be at least the diameter of the bubble divided by forty, then simulations could be used as an investigative tool for studying a single bubble rise, and the balance between accuracy and time execution is adequate. Once, IsoAdvector was the solver elected, two cases from the Krishna et al. (1999) article [8] were simulated, one in two dimensions and the other in three dimensions. The simulations cover a range of bubble between 4 and 12 millimeters in diameter. The two dimensions results were compared with experimental, simulated and numerical data base of Krishna et al. (1999) [8]. These simulations are in close agreement with that data base, in which the simulations were computed with the commercial software ANSYS-CFX. An algorithm implemented in Matlab was developed to compute the rise velocities and it worked really well: the maximum different between the rise velocities was only a five percent, see Table 7. The trajectories and bubble shapes match quite well with those shown in Article [8]. The main conclusion extracted for those simulations is that the maximum magnitude of the lateral migration and the frequency of a bubble can be predicted in the studied range, but the direction of the bubble is random, see Figure 27.

After those simulations, three dimensions simulation were carried out. The results, also match with the experimental data shown in Articles [8] and [10], equation proposed by Jamialahmadi JM. et al. (1994) [9] and simulations shown by Manoj Kumar Tripathi et al. (2015) [5], see 10. Additionally, bubble shapes are in close agreement with those shown in [5], see Figures from 35 to 37. Although some 3D shapes match with real images, however, it is needed more literature to validate the entire range simulated, see Figures from 39 to 42. Similar to two dimensions results, the highest error in rise velocities is less than the six percent, see Table 10. It was proved that IsoAdvector is able to run proper simulations without an hexahedral mesh, see Figure 33. Finally, it was checked that the simulations computed represented distilled water and the experiments done in [8] were carried out with tap water, in accordance with the difference between rise velocities, about an eight or twelve percent, see Table 10.

Therefore, the main results of the thesis consist of the following observations:

- IsoAdvector algorithm runs much better than MULES algorithm and it works proper in non-hexahedral meshes.

- Grid accuracy should be at least the diameter of the bubble divided by forty, then balance between accuracy and time execution is adequate.
- The simulation results are in close agreement with the theoretical, experimental and computational literature.
- The maximum magnitude of the lateral migration and the frequency of a bubble can be predicted, but the direction of the bubble is random.
- 2D bubble shape are not match with the projection of real ones, however it may be established a relation between 2D and 3D shapes.
- A few real photographs were found in the literature and successfully compared with the present study results, in terms of bubble shape, nevertheless it is hoped that there will be more experiments of this class to check the simulations present here.

Concerning future works, direct numerical simulations (DNS) of bubbly flows with heat transfer should be treated. In addition, this is a field which is still relatively rare, due to the majority of the simulations are about single-phase flows and there are a great amount of discrepancies between them, such as the nucleation of bubble and the change in the volume because of the pressure, temperature and mass of bubbles. The few publications found regarding heat transfer in bubbly flows in vertical channels, here only three publications [69], [70] and [71] are aware, assert that the presence of bubbles and droplets generally increases the local heat transfer, but, they also increment the wall friction. However, it depends on the bubble shape: nearly spherical bubbles increases the wall friction, whereas more distorted bubbles mostly affect the flow rate by reducing the density of the mixture, since they typically stay away from the walls.

Annex

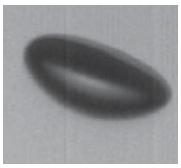

(a) Source [72]

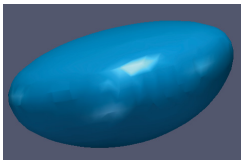

(b) Source: Present study

Figure 39: Bubble shapes.

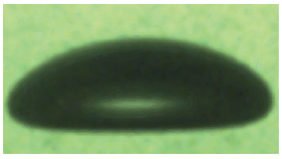

(a) Source [73]

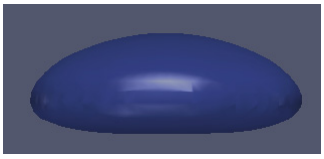

(b) Source: Present study

Figure 40: Bubble shapes.

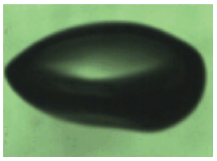

(a) Source [73]

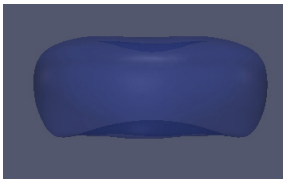

(b) Source: Present study

Figure 41: Bubble shapes.

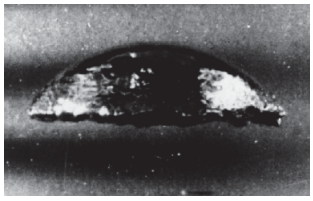

(a) Source [11]

(b) Source: Present study

Figure 42: Bubble shapes.

References

[1] *Handbook of Fluids in Motion*, chapter Hydrodynamics of bubble columns. Ann Arbor Science, 1983.

[2] Blandín-Arrieta J. Visualización y descripción de la dinámica de burbujas. Master's thesis, Chemical Engineering, Universidad Autónoma Metropolitana, Iztapalapa, Mexico, 1997.

[3] Shaobai Li1, Shuang Xul, Zheng Yanl, Rundong Lil, and Tianhua Yangl. The formation behavior of a single bubble in power-law fluids. *Brazilian Journal of Chemical Engineering*, 34, 2017.

[4] R Clift, J.R. Grace, and M.E. Weber. *Bubbles, drops and particles*. Academic Press, San Diego, 1978.

[5] Manoj Kumar Tripathi, Kirti Chandra Sahu, and Rama Govindarajan. Dynamics of an initially spherical bubble rising in quiescent liquid. *Nature communications*, pages 1–9, February 2015.

[6] S. Baz-Rodríguez, A. Aguilar-Corona, and A. Soria. Rising velocity for single bubbles in pure liquids. *Revista Mexicana de Ingeniería Quimica*, 11, 2012.

[7] Johan Roenby, Henrik Bredmose, and Hrvoje Jasak. A computational method for sharp interface advection. In *Royal Society Open Science*, volume 3. 2016.

[8] R. Krishna and J.M. van Baten. Rise characteristics of gas bubbles in a 2d rectangular column: Vof simulations vs experiments. *International Communications in Heat and Mass Transfer*, 26(7):965–974, 1999.

[9] Jamialahmadi JM., Branch, and Muller-Steinhagen H. Terminal bubble rise velocity in liquids. In *Chemical Engineering Research and Design*, volume 72, pages 119–122. 1994.

[10] Kamil Wichterle, Kateřina Smutná, and Marek Večeř. Shape and rising velocity of bubbles. In J. Markoš, editor, *36th International Conference of Slovak Society of Chemical Engineering*, May 2009.

[11] *Fundamentals of Multiphase Flows*. Cambridge University Press 2005, California Institute of Technology, Pasadena, California, 2008.

[12] C. Peña-Monferrer, G. Monrós-Andreu, S. Chiva, R. Martínez-Cuenca, and J.L. Muñoz Cobo. A cfd-dem solver to model bubbly flow. part ii: Critical validation in upward vertical pipes including axial evolution. In *Chemical engineering science*, volume 177, pages 537–556. 2018.

[13] Roland Rzehak and Sebastian Kriebitzsch. Multiphase cfd-simulation of bubbly

pipe flow: A code comparison. *International Journal of Multiphase Flow*, 68:135–152, November 2014.

[14] Rosemary Sugrue, Ben Magolan, Nazar Lubchenko, and Emilio Baglietto. Assessment of a simplified set of momentum closure relations for low volume fraction regimes in star-ccm+ and openfoam. *Annals of Nuclear Energy*, 110:79–87, June 2017.

[15] R Collins. A simple model of the plane gas bubble in a finite liquid. *Fluid Mechanics*, 22:763–771, 1965.

[16] W.L. Haberman and R.K. Morton. An experimental investigation of the drag and shape of air bubbles rising in various liquids. Technical report, Technical library, US Department of the NAvy, Washington, DC., 1953.

[17] *Jets, Wakes, and Cavities*. Academic Press, 1957.

[18] Marshall P. Tulin. Suprcavitating flows - small-perturbation theory. *Journal of Ship Research*, 7(3):16–37, 1964.

[19] L.C. Woods. Theory of subsonic plane flow. *The Aeronautical Journal*, 1961.

[20] T.Y. Wu. Cavity and wake flows. *Journal in Fluid Mechanics*, 4:243–284, 1972.

[21] Jones O.C. and Zuber N. Statistical methods for measurement and analysis of two-phase flow. In *Proceeding of International Heat Transfer Conference*, Tokyo, 1974.

[22] Takashi Yasuda, Noriyuki Takahashi, Masafumi Baba, Kazuyoku Tei, and Shigeru Yamaguchi. An experimental study on micro-bubble generation by laser-induced breakdown in water. Technical report, Department of Physics, School of Science,, Tokai University, 1117 Kitakaname, Hiratsuka 259-1292, 2008.

[23] Morteza Gharib and Mingming Wu. Experimental investigations on the bistable shape states of small air bubbles rising in clean water. Technical report, California Institute of Technology, 2001.

[24] Gholamreza Keshavarzi, Ryan S. Pawell, Tracie J. Barber, and Guan H. Yeoh. Transient analysis of a single rising bubble used for numerical validation for multiphase flow. In *Chemical Engineering Science*. 2014.

[25] R. Kumar, R. Ramakrishnan, and N.R. Kuloor. Studies in bubble formation 1. bubble formation under constant flow conditions. In *Chemical Engineering Science*, volume 24, pages 731–747. 1969.

[26] E.S. Gaddis and A. Vogelpohl. Bubble formation in quiecent liquids under constant flow conditions. In *Chemical Engineering Science*, volume 41, pages

97–105. 1986.

[27] E.T. White and R.H. Beardmore. The velocity of rise of single cylindrical air bubbles through liquids contained in vertical tubes. In *Chemical Engineering Science*, volume 17. 1962.

[28] *Bubble Rising Velocity in Saturated Liquid up to Critical Pressure*. Experimental Heat Transfer, Fluid Mechanics and Thermodynamics, 2001.

[29] B. Rosenberg. The david w.taylor model basin. Technical Report 727, Washington : U.S. Experimental Model Basin, Navy Yard, 1950.

[30] A.W.G de Vries. *Path and Wake of a Rising Bubble*. PhD thesis, University of Twente, 2001.

[31] Bagha D. and Weber M.E. Bubbles in viscous liquids: shapes, wakes and velocities. *Journal of Fluid Mechanics*, pages 61–85, April April 2006.

[32] *Fluid Dynamics of Cavitation and Cavitating Turbopumps*, chapter The Rayleigh-Plesset equation: a simple and powerful tool to understand various aspects of cavitation. Springer Wien New York, University of Grenoble, France, 2007.

[33] Matias Ignacio Inaipil Leal. Anlasis fluido dinamico de un flujo de burbujas mediante cfd. Master's thesis, School of Physics and Mathematics, Santiago de Chile, 2015.

[34] J.R. Grace and D. Harrison. The influence of bubble shape on the rising velocities of large bubbles. In *Chemical Engineering Science*, volume 22, pages 1337–1347, 1967.

[35] K. Tsuchiya and L. Fan. Near-wake structure of a single gas bubble in a two-dimensional liquid-solid fluidized bed: Vortex shedding and wake size variation. In *Chemical Engineering Science*, volume 43, pages 1167–1181, 1988.

[36] R. Collins. The cycloidal-cap bubble: A neglected solution in the theory of large plane gas bubbles in liquids. In *Chemical Engineering Science*, volume 22, pages 88–97, 1967.

[37] J. Berghmans. Stability of large two-dimensional gas bubbles. In *Chemical Engineering Science*, volume 29, pages 1645–1650, 1974.

[38] Moore D.W. The boundary layer on a spherical gas bubble. *Journal of Fluid Mechanics*, 16:161–176, 1963.

[39] Lehrer I.H. A rational terminal velocity equation for bubbles and drops at intermediate and high reynolds numbers. *Journal of Chemical Engineering of Japan*, 9:237–240, 1976.

[40] Role of Mach Number in Compressible Flows. `https://www.grc.nasa.gov/www/k-12/airplane/machrole.html`, May 05 2015.

[41] C.W. Hirt and B.D. Nichols. Volume of fluid (vof) method for the dynamics of free boundaries. *Computational Physics*, 39:201–225, 1981.

[42] Edin Edin Berberovic, Nils P. van Hinsberg, Suad Jakirlic, Ilia V. Roisman, and Cameron Tropea. Drop impact onto a liquid layer of finite thickness: Dynamics of the cavity evolution. Technical report, Technische Universität Darmstadt, Chair of Fluid Mechanics and Aerodynamics, 2009.

[43] *Nonlinear Water Wave Interaction.* WIT Press Computational Mechanics Publications, 1999.

[44] R. Scardovelli and S. Zaleski. Direct numerical simultaion of free-surface and interfacial flow. In *Annual Review of Fluid Mechanics*, volume 32, pages 567–603. 1999.

[45] S. Afkhami and M. Bussmann. Height functions for applying contact angles to 2d vof simulations. *International Journal for Numerical Methods Fluids*, 57, 2008.

[46] S. J. Cummins, M. M. Francois, and D. B. Kothe. Estimating curvature from volume fractions. *Computers and Structures*, 83, 2005.

[47] Henrik Rusche. *Computational Fluid Dynamics of Dispersed Two-Phase Flows at High Phase Fractions.* PhD thesis, Imperial College of Science, Technology and Medicine, London, 2002.

[48] Akio Tomiyama, Iztok Zun, Akira Sou, and Tadashi Sakaguchi. Numerical analysis of bubble motion with the vof methods. *Nuclear engineering and design*, 141:69–82, 1993.

[49] Krishna R, J.M. van Baten, M.I. Urseanu, and J. Ellenberger. Rise velocity of single circular-cap bubbles in two-dimensional beds of powders and liquids. *Chemical Engineering and Processing*, 39:433–440, 2000.

[50] H.K. Versteeg and W. Malalasekera. *An introduction to Computational Fluids Dynamics.* Longman scientific and technical, 1995.

[51] Joel H. Ferziger and Milovan Peric. *Computational Methods for Fluid Dynamics.* Springer, 1995.

[52] H. Jasak. *Error Analysis and Estimation for the Finite Volume Method with Applications to Fluid Flows.* PhD thesis, Imperial College of Science, Technology and Medicine, London, 1996.

[53] Suraj S. Deshpande, Lakshman Anumolu, and Mario F. Trujillo. Evaluating the performance of the two-phase flow solver interfoam. *Computational Science Discovery*, 5, 2012.

[54] Johan Roenby1, Henrik Bredmose, and Hrvoje Jasak. Isoadvector: Free, fast and accurate vof on arbitrary meshes. In 4^{th} *OpenFOAM User conference*, 2016.

[55] Santiago Márquez Damián. *An Extended Mixture Model for the Simultaneous Treatment of Short and Long Scale Interfaces*. PhD thesis, FICH and INTEC, Santa Fe, Argentina, 2013.

[56] Tobias Holzmann. *Mathematics, Numerics, Derivations and OpenFOAM®*. Holzmann CFD, December 2016.

[57] R.I. Issa. Solution of the implicitly discretised fluid flow equations by operator-splitting. *Jpurnal of Computational Physics*, 62:40–65, January 1986.

[58] Gerald C.J. Morgan. Appplication of the interfoam vof code to coastal wave/structure interaction. Master's thesis, University of Bath Department of Architecture and Civil Engineering, February 2013.

[59] Pedro Miguel Borges Lopes. Free-surface flow interface and air-entrainment modelling using openfoam. Master's thesis, Hydraulic, Water Resources and Environment Doctoral Program in Civil Engineering, August 2013.

[60] Fadl Moukalled, Marwan Darwish, and Luca Mangani. *The Finite Volume Method in Computational Fluid Dynamics An Advanced Introduction with OpenFOAM® and Matlab (Fluid Mechanics and Its Applications)*, volume 113. Springer-Verlag, 2015.

[61] *Numerical Methods in Fluid Dynamics*, chapter Time-Dependent Multi-material Flow with Large Fluid Distortion, pages 273–285. Academic Press, Jaunary 1982.

[62] Meng Huang, Lilong Wu, and Bin Chen. A piecewise linear interface-capturing volume-of-fluid method based on unstructured grids. *International Journal of Computation and Methodology*, 61:418–425, 2012.

[63] Johan Roenby, Henrik Bredmose, Hrvoje Jasak, and Bjarke Eltard Larsen. A new volume-of-fluid method in openfoam. *VII International Conference on Computational Methods in Marine Engineering*, 2017.

[64] Alessandro Manni. An introduction to twophaseeulerfoam with addition of an heat exchange model. Master's thesis, Chalmers University of Technology, 2014.

[65] Hadamard J. Mouvement permanent lent d'une sphère liquide et visqueuse dans un liquide visqueux. *Comptes Rendus de l'Académie des Sciences*, pages

1735–1752, 1911.

[66] Christopher J. Greenshields. *OpenFoam User Guide*, volume Version 5.0. OpenFOAM foundation Ltd, July 2017.

[67] Sancak Özdemir. *Investigation of air bubble motion in water through a vertical narrow rectangular channel by using image processing techniques in mechanical engineering.* PhD thesis, Natural and applied sciences of middle east technical university, August 2005.

[68] Liang Shih Fan and Katsumi Tsuchiya. *Bubble Wake Dynamics in Liquids and Liquid-Solid Supensions.* Butterworth Heinemann Series in Chemical Engineering., Boston, 1990.

[69] Sadegh Dabiri and Gretar Tryggvason. Heat transfer in turbulent bubbly flow in vertical channels. In *Chemical Engineering Science*. 2014.

[70] *Computational Simulations and Applications*, chapter Numerical study on flow structures and heat transfer characteristics of turbulent bubbly up flow in a vertical channel, page 119–142. IntechOpen, 2011.

[71] Lu J. and Tryggvason G. Effect of bubble deformability in turbulent bubbly up flow in a vertical channel. In *Physics of Fluids*. 2008.

[72] Mingming Wu and Morteza Gharib. Experimental studies on the shape and path of small air bubbles rising in clean water. In *Physics of Fluids*, volume 14. American Institute of Physics, 2002.

[73] Liu Liu, Hongjie Yan, and Guojian Zhao. Experimental studies on the shape and motion of air bubbles in viscous liquids. *Experimental Thermal and Fluid Science*, 2014.

[74] Peebles F. N. and Garber H. J. Studies on the motion of gas bubbles in liquids. In *Chemical Engineering Progress*, volume 49, pages 88–97. 1953.

[75] Okazaki S. The velocity of ascending air bubbles in aqueous solutions of a surface active substance and the life of the bubble on the same solution. In *Bulletin of the Chemical Society of Japan*, volume 37, pages 144–150. 1964.

[76] Aybers N. M. and Tapucu A. The motion of gas bubbles rising through stagnant liquid. In *HEat and Mass Transfer*, volume 2, pages 118–128. 1969.

[77] Leifer I., Patro R. K., and Bowyer P. A study on the temperature variation of rise velocity for large clean bubbles. *Journal of Atmospheric for large clean bubbles*, pages 1392–1402, 2000.

[78] Okawa T., Tanaka T., Kataoka I., and Mori M. Temperature effect on single bubble rise characteristics in stagnant distilled water. *International Journal of*

Heat and Mass Transfer, 46:903–913, 2003.

[79] Talaia M.A.R. Terminal velocity of a bubble rise in a liquid column. In *Proceedings of the World Academy of Science, Engineering and Technology*, volume 22, pages 264–268, 2007.

[80] Rodrigue D. Generalized correlation for bubble motion. *AIChE Journal*, 47:39–44, 2001.

[81] R. Collins. The effect of a containing cylindrical boundary on the velocity of a large gas bubble in a liquid. *Journal of Fluid Mechanics*, 28:97–112, 1967.

[82] *Numerical Computation of internal and external flows.* Elsevier Ltd, 1991.